621.06
JA
V. 3

BULLETIN OF JAPAN SOCIETY OF GRINDING ENGINEERS

UNIVERSITY OF
DEC 29 1965
LIBRARY

1963
JAPAN SOCIETY OF GRINDING ENGINEERS
Vol. 3

REGULATION OF JAPAN SOCIETY OF GRINDING ENGINEERS (EXTRACTED). Dec. 1963

1. Japan Society of Grinding Engineers, founded in 1956, consists of the researchers and engineers who take interest in precision machining by the aid of abrasive grains and wheels including diamond. Our Society is now a center of researches of abrasive machining in Japan.

   The works to be perfomed by the Society are ranged as follows:

   (1) abrasive grains, (2) diamond, (3) grinding wheels, (4) diamond wheels, (5) abrasive belts, (6) grinding fluids, (7) grinding, (8) abrasive belt grinding, (9) honing, (10) super-finishing, (11) lapping, (12) buffing, (13) barreling, (14) blasting, (15) ultrasonic machining, (16) qualities of abrasive machined surfaces. Theories, techniques and machines are included in each items.

2. Activities till December, 1963 from 1956.

   (1) 84 issues of journal including 330 papers were published monthly written in Japancese as "Journal of Japan Society of Grinding Engineers."

   (2) Monthly meeting were held 86 times and 180 research papers were presented.

   (3) About 2260 foreigh papers concerning above 16 items were digested in our journals.

   (4) Investigations of practical shops were held 28 times and contributed to the progress of abrasive machining techniques in praitical shops.

   (5) Symposeums on the special items were held 13 times as the following: (i) cutting mechanism of a grain, (ii) grinding fluids (three times). (iii) ceramic tools, (iv) abrasive grains (twice), (v) resinoid wheels, (vi) diamond, (vii) grinding techniques in Europe, U.S.A, and U.S.S.R. (three times), (viii) grade of grinding wheels.

   (6) English journal were published from 1961 once a year as "Bulletin of Japan Society of Grinding Engineers." 23 papers were published in Vol.1 1961, 7 papers in Vol 2, 1962,

3. Members:

   (1) Honored members: 2 in Japan and 4 in other countries,

   (2) Members who belonged to universities: 53 peoples covers 26 universities.

   (3) Members who belonged to governmental laboratories: 40 peoples covers 10 laboratories,

   (4) Members who belonged to factories: 294 peoples covers 267 companies.

4. Officials:

   Chairman

   Secretary

   Account auditor

   Executive managers

5. Location of the Office.

   Electrotechnical Laboratory, MITI.

   Ginza-Higashi 8-19, Chuo-ku, Tokyo, Japan.

With the Author's Compliments

Features and Principles of Through Wheel Coolant Grinding

By

Kenji SATO

Reprinted from
The Technology Reports of the Tohoku University,
Vol. XXVIII (1963) No. 1

Digitized by the Internet Archive
in 2025 with funding from
University of Illinois Urbana-Champaign Alternates

https://archive.org/details/bulletinofjapans3196japa

Features and Principles of Through Wheel Coolant Grinding

By

Kenji SATO*

Synopsis

Through wheel coolant grinding is a novel method for lowering the grinding temperature and preventing the grinding burn. It was found that soybean oil was the most effective of through wheel coolants owing to its lowest coefficient of friction in grinding. The principle of cooling seems to be the evaporation of mist oil which reaches the wheel work contact surface through the pores of the grinding wheel.

1. Introduction

As seen from the spark in grinding operation, the grinding temperature is exceedingly high and the work piece reaches a considerably high temperature. Therefore, it is very important to cool the grinding point with plentiful liquid. Though grinding fluid is poured usually on the wheel-work interface, the fluid, in severe grinding conditions, becomes insufficient and occationally grinding burn appears.

In such cases, through wheel coolant grinding is the most effective. This is a novel cooling method, in which the coolant is supplied at the center part of a grinding wheel and, through the pores of the wheel, it sprays out of the wheel periphery by centrifugal action. The mist of the coolant which enters into the grinding point improves the cooling efficiency so much that only a little amount of coolant will serve.

The first practical example of this method is a surface grinder made nearly in 1950 by Do-All Company in USA as shown in Fig. 1. It is named "cool grinding", and it has many good features, such as, lowering grinding temperature, decreasing wheel wear, improving surface roughness, that the contact point of grinding wheel and the work can be observed accurately, and that chips are prevented from scattering. This idea, however, is not new. It is reported that an American named W. Cavert got his American patent early in 1888[1], and now it is known to everyone.

In Japan, Sasaki and others[2] gave some data on the effect of through wheel coolant grinding. They compared the grinding resistances between through wheel

* Professor of Precision Engineering.

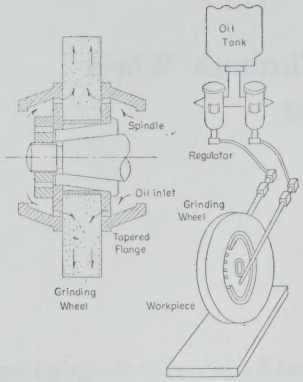

Fig. 1. Do-All Cool Grinding

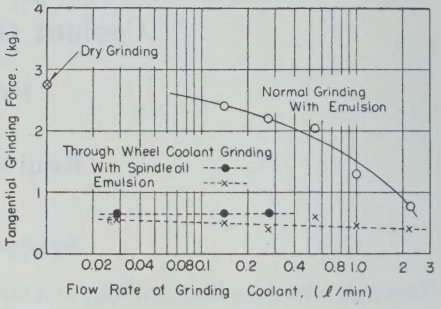

Fig. 2. Decrease of Grinding Force by Through Wheel Coolant Grinding

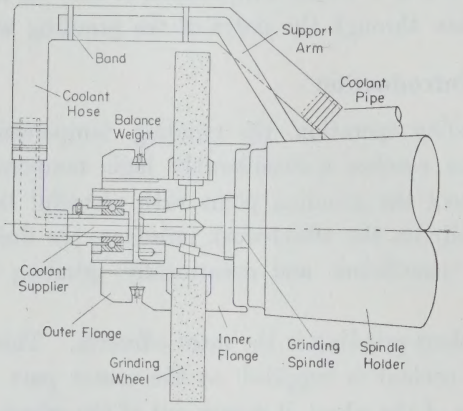

Fig. 3. Through Wheel Coolant Grinding Applied to Internal Grinding

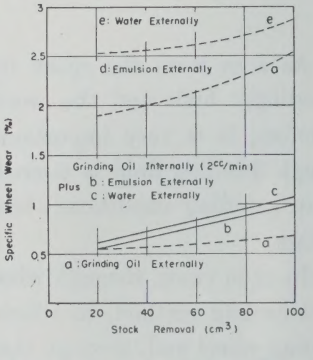

Fig. 4. Specific Wheel Wear in Through Wheel Coolant Grinding

coolant grinding and normal wet grinding. One of the results, in Fig. 2, showed clearly lower resistance of through wheel coolant grinding, even when the flow rate of coolant was only 30cc/min.

An industrial application of this method to internal grinding was performed at Yokohama Shipyard of Mitsubishi-Nihon Heavy Industries Co.[3] A cast iron cylinder of a marine diesel engine having a bore of 300 mm was ground with an apparatus shown in Fig. 3. The results were reported as follows:

(1) Grindability was improved even when harder grinding wheels than normal were used, and the number of pieces per dressing increased.

(2) Depth of grinding could be increased owing to the lower grinding temperature, and the accuracy of work pieces increased on account of decreased surface strain.

(3) Surface finish was better than by dry grinding.

(4) Grinding wheels were apt to loaded with sludge when coolant was used circularly. A coolant filter made of vinylsponge was used with satisfactory results in this case.

In West Germany, 1954, Pahlitzsch[4] recommended "the two-way coolant device", in which grinding oil was fed through wheel and emulsified grinding coolant was poured externally in the normal way. Specific wheel wear decreased remarkably when internally fed grinding oil was only 2cc/min., as shown in Fig. 4.

Though the through wheel coolant method is performed successfully in several places as mentioned above, the mechanism of cooling by this method is yet unknown. The object to be aimed at in this paper is to clarify the effects of this method and the mechanism of cooling.

2. Experimental Apparatus for Through Wheel Coolant Grinding[5]

The schematic arrangement of the apparatus is shown in Fig. 5. A bench type tool grinder, fitted with a bevel gear torque-meter, was used. Test pieces were pushed against the periphery of the grinding wheel with varying dead load. Coolant was stored in a tank, and then it sprayed out of the wheel periphery through pores.

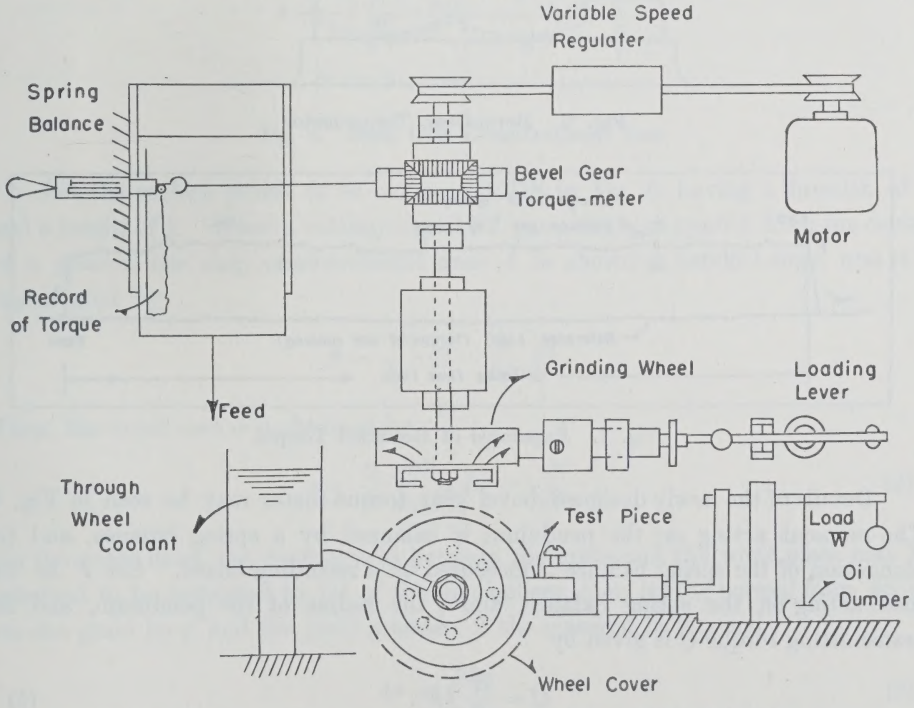

Fig. 5. Experimental Apparatus for Through Wheel Coolant Grinding

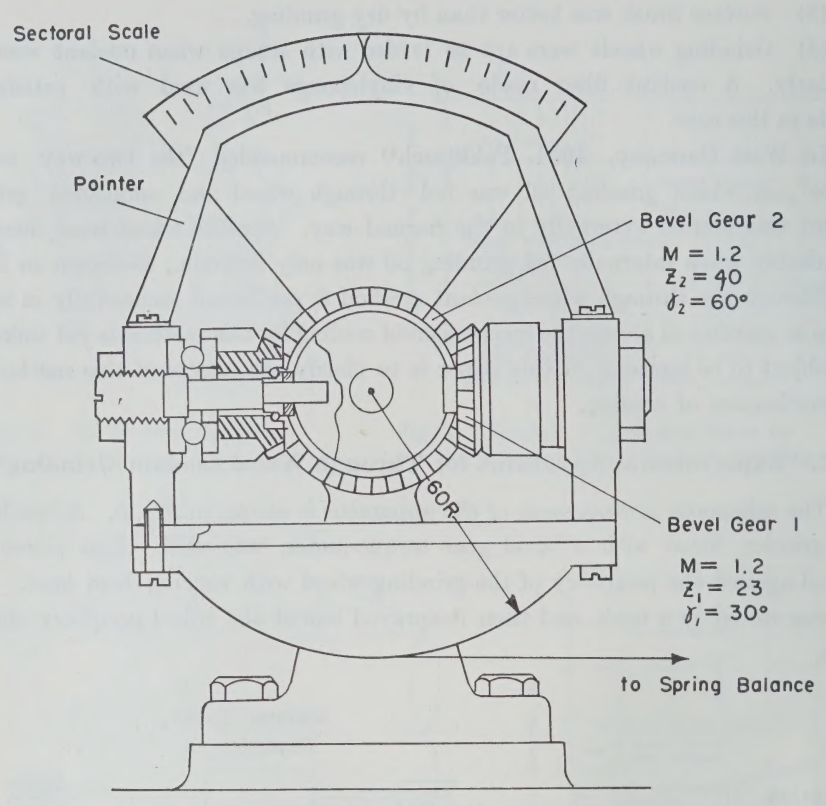

Fig. 6. Bevel-Gear Torquemeter

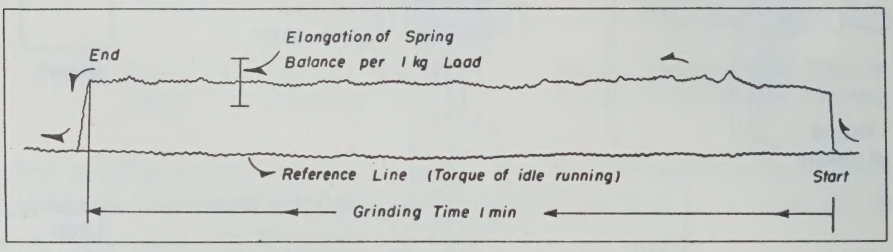

Fig. 7. Expample of Recorded Torque.

Details of the newly designed bevel gear torque-meter may be seen in Fig. 6. The moment acting on the pendulum is balanced by a spring balance, and the elongation of the spring balance is measured on a recording board. Let F be the force acting on the spring balance, and l the radius of the pendulum, and the transmitting torque Q is given by

$$Q = \frac{1}{2} l F . \tag{1}$$

One of the records is shown in Fig. 7, and the force F is determined by measuring the area enclosed by the recorded line and the reference line. The accuracy of measured grinding force is of the order of 0.01 kg.

Test pieces were made of annealed or hardened carbon tool steel and hardened high speed steel. Water, emulsion, kerosene, and soybean oil were used as grinding coolants. By varying the wheel speed and the grinding pressure, the stock removal and the grinding force were measured.

3. Grinding Efficiency and Grinding Force

3-1 Stock Removal in Plunge-Cut Grinding

A theoretical calculation for the stock removal in plunge-cut grinding is performed, presuming that each cutting edge of the grinding wheel acts as a hemisphere having a radius of r, and grooves formed on the workpiece have the same radius r, no account being taken then of elastic recovery of the workpiece and random arrangement of the cutting edge.

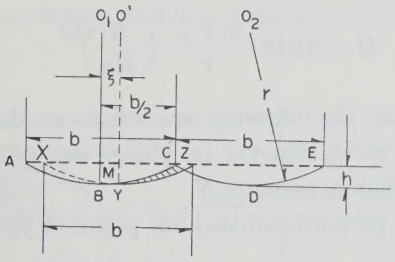

Fig. 8. Mean Chip Cross-Sectional Area

Let the surface profile to be cut be ABCDE in Fig. 8, having a breadth of b and a height of h. When a cutting edge XYZ passes a point apart ξ from the center of a groove, the chip cross-sectional area A is shown as hatched zone, and it is represented by

$$A = \frac{b^2}{8r}\xi - \frac{b}{8r}\xi^2 .$$

Then, the mean area a is obtained by

$$a = \frac{2}{b}\int_0^{b/2} A\, d\xi = \frac{b^3}{48r} . \tag{2}$$

On the other hand, the contact area between the grain and the work piece may be assumed to be restricted to 1/4 of the hemisphere, then let the normal force acting on one grain be q, and the yield pressure of the material be p_m, and

$$b^2 = \frac{16q}{\pi p_m} . \tag{3}$$

If the total grinding pressure is N, q is expressed by

$$q = N w^2 , \tag{4}$$

where w is mean grain spacing.

The weight of chips removed per unit area M is given by

$$M = \rho \frac{a}{w^2} V , \tag{5}$$

where V is the grinding speed, and ρ is the density of the chip.

Putting the equations (2), (3), and (4) into (5), we get a formula representing the stock removal weight M in definite parameters except the radius r:

$$M = \frac{4}{3\pi\sqrt{\pi}} \frac{w V \rho}{r} \left(\frac{N}{p_m}\right)^{1.5} . \tag{6}$$

Instead of the yield pressure p_m, we may use Vickers hardness Hv. From the relation $p_m = 1.08\, Hv$, the following is obtained:

$$M = 0.213 \frac{w V \rho}{r} \left(\frac{N}{Hv}\right)^{1.5} . \tag{7}$$

From these equations, the following conclusions are derived:

(1) The weight of stock removal in plunge-cut grinding M is proportional to 1.5th power of the grinding pressure N.

(2) M is inversely proportional to 1.5th power of yield pressure p_m or Vickers hardness Hv.

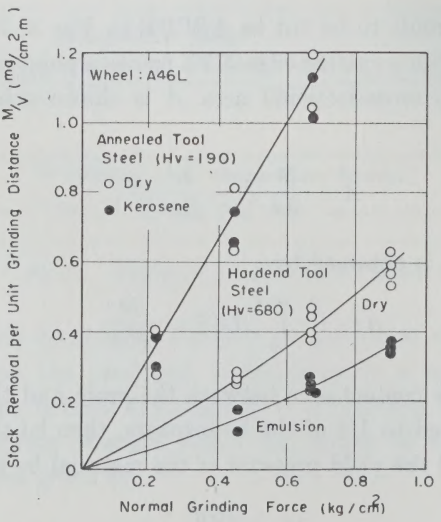

Fig. 9. Specific Stock Removal versus Grinding Pressure in Plunge-Cut Grinding

(3) M is proportional to the mean grain spacing w. Generally a wheel of coarse grain and wide structure has a better grinding efficiency.

(4) M is inversely proportional to the radius of cutting edge r. This means that a wheel having better cleavability removes more stock from the workpiece, and a glazed wheel gives less stock removal.

An experimental verification of those formulae is shown in Fig. 9, where a wheel of A46L grinds hardened and annealed carbon tool steel in the cases of dry grinding and through wheel coolant grinding.

Another experiment where annealed carbon steel test-pieces are ground by a A46N wheel with various through wheel coolants is performed. Measured stock removal and grinding forces, and calculated specific grinding energy are shown in Fig. 10. It is clear that soybean oil is the most effective owing to its high stock removal and low grinding force, resulting in extremely low specific grinding energy. The mean values of specific grinding energy in this experiment are shown in Table 1. The data of soybean oil are about half of those in dry grinding. This owes much to the reduced friction force between the cutting grain and the workpeice. The same effect is obtained when stearic acid 5% in machine oil is used as through wheel coolant.

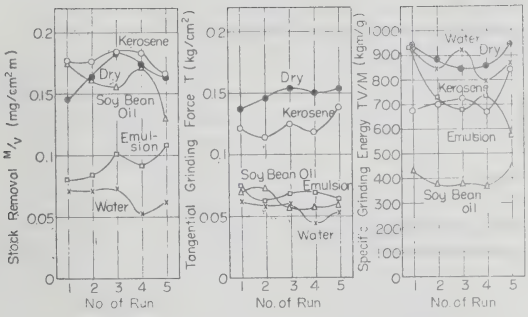

Fig. 10. Stock Removal, Tangential Grinding Force, and Specific Grinding Energy With Various Through Wheel Coolants

Table 1. Specific Grinding Energy (TV/M) With Various Through Wheel Coolants

Coolant	Soybean oil	Kerosene	Emulsion	Water	Dry
$\left(\frac{TV}{M}\right)$ in kg·m/g	403	728	733	878	897
in cal/g	945	1710	1720	2060	2100

3-2 Grinding Force in Plunge-Cut Grinding and Coefficient of Friction in Grinding

It is generally recognized that the tangential grinding force T consists of two parts, namely the chip shearing term T_a and the friction term μN, where μ is the

coefficient of friction in grinding and N is the normal grinding force. That is,

$$T = T_a + \mu N . \tag{8}$$

Suppose T_a is the product of the specific grinding force σ and the mean chip sectional area a multiplied by the number of cutting edges n, and also σ is represented by

$$\sigma = \sigma_0 \left(\frac{a_0}{a} \right)^{\nu} . \tag{9}$$

from the size effect of chip area. Then

$$T_a = \sigma a n = n \sigma a_0^{\nu} \cdot a^{(1-\nu)} . \tag{10}$$

In plunge-cut grinding by a definite grinding wheel, as shown in the equation (5),

$$a \propto (M/V) . \tag{11}$$

Finally, the equation (8) may be rewritten by the following:

$$T = \mu N + k (M/V)^{(1-\nu)} , \tag{12}$$

where k is a constant represented by the next equation,

$$k = \frac{\sigma_0 (a_0 n)^{\nu}}{\rho^{(1-\nu)}} . \tag{13}$$

Accordingly, when the values of T and M/V are measured in plunge-cut grinding

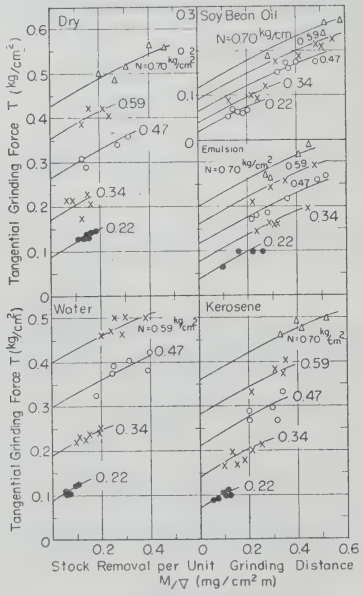

Fig. 11. Tangential Grinding Force versus Stock Removal per Unit Grinding Distance (1), Data of Annealed Carbon Steel With A46N Wheel.

experiments with varying N and V, the values of μ, ν and k can be determined by the equations (12) and (13).

The grinding experiments were performed by applying 10cc/min of various coolants: water, emulsion, kerosene and soybean oil, and air for comparison. The data of annealed carbon steel with a A46N wheel are shown in Fig. 11, and those of hardened high speed steel with a A46H wheel are shown in Fig. 12.

Most of the points in the figures lie along curves having parameters of the

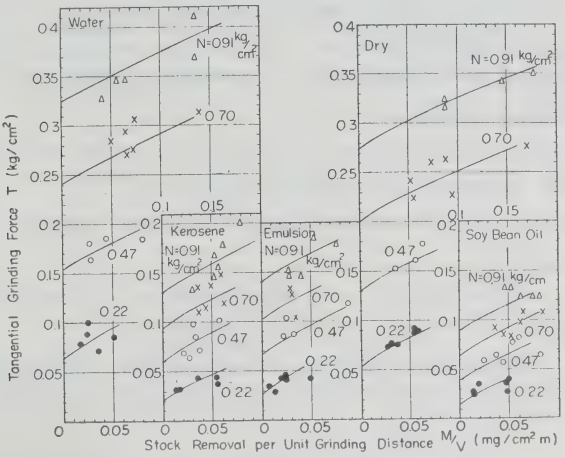

Fig. 12. Tangential Grinding Force versus Stock Removal per Unit Grinding Distance (2), Data of Hardened High Speed Steel With A46H Wheel.

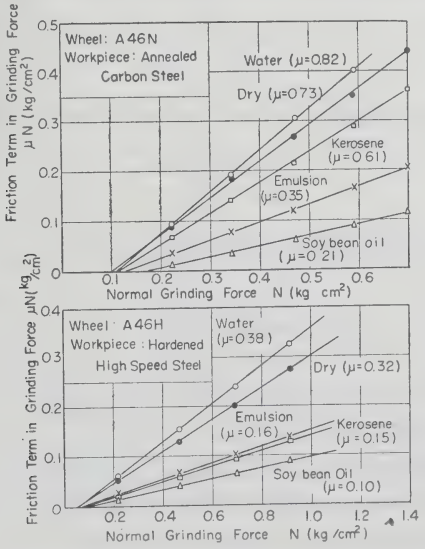

Fig. 13. Determination of Coefficient of Friction in Grinding

Table 2. Coefficient of Friction in Grinding

Coolant	Soybean oil	Kerosene	Emulsion	Water	Dry
Annealed Carbon Steel	0.21	0.61	0.35	0.82	0.73
Hardened High Speed Steel	0.10	0.15	0.16	0.38	0.32

normal grinding force N. If the curves are extended to the left, the intersecting points with the ordinate where the ratio M/V is zero, represent the friction term μN. According to the plots between μN and N, as shown in Fig. 13, the coefficient of friction in grinding μ can be determined. The values are listed in Table 2. The following conclusions are obtained:

(1) The coefficient of friction in grinding with hardened high speed steel is about half as much as that with annealed carbon steel.

(2) In the case of water, the coefficient of friction is slightly higher than in the case of dry grinding.

(3) Emulsion and kerosene are good lubricants, reducing the coefficient of friction considerably.

(4) Soybean oil is the most effective one, the coefficient of friction being about one third of that in dry grinding. The heat generated in grinding, therefore, is less, and the surface finish is much better.

3-3 Specific Shear Energy and Rate of Shearing Term in Grinding Force[6]

From the data mentioned above, the force required to shear off chips T_a can be obtained by

$$T_a = T - \mu N . \tag{14}$$

Then, the specific shear energy E_s may be calculated by the following equation:

$$E_s = \frac{T_a \times V}{M} . \tag{15}$$

Since the mean chip cross-sectional area a can be given by

$$a = \frac{M}{V} \cdot \frac{w^2}{\rho} , \tag{16}$$

where w is the mean spacing of cutting edges, the relation between E_s and a can be plotted as shown in Fig. 14.

Though the points scatter considerably, it is concluded from the mean curves that the specific shear energy is 250～300 kg-m/g in the case of annealed carbon steel, and 500～600 kg-m/g in the case of hardened high speed steel.

The specific shearing force in grinding σ, which is the shearing force per unit

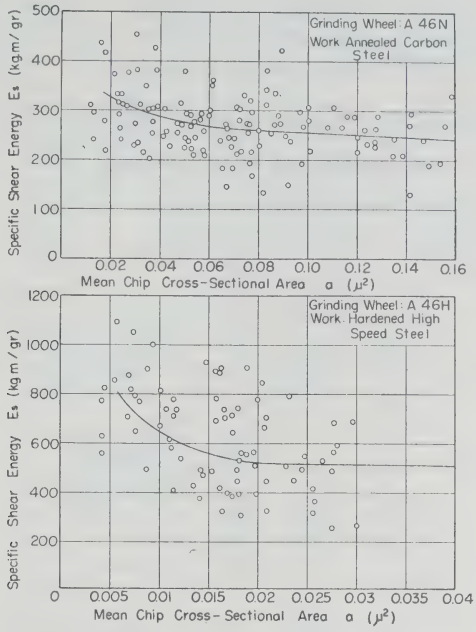

Fig. 14. Specific Shear Energy versus Mean Chip Cross-Sectional Area

cross-sectional chip area, can be calculated by the equation

$$\sigma = \frac{T_a}{a \cdot n} . \tag{17}$$

By plotting the data of σ and a in logarithmic scales, the following experimental formulae can be obtained:

Annealed carbon steel:

$$\sigma = 1.56\,(a)^{-0.104} \times 10^3\ \mathrm{kg/mm^2} \quad (a \text{ in } \mu^2 \text{ unit}) .$$

Hardened high speed steel:

$$\sigma = 3.02\,(a)^{-0.073} \times 10^3\ \mathrm{kg/mm^2} \quad (a \text{ in } \mu^2 \text{ unit}) .$$

In the regions of experimental conditions, with annealed carbon steel σ is about 2000 kg/mm² where a is 0.1 μ^2, and with hardened high speed steel σ rises up to 4000kg/mm² where a is 0.02μ^2. These values of the specific shearing force in grinding are exceedingly high, and they will be the fundamental data relating to the size effect in fracture of metals and to the inter-atomic strength of perfect metals without dislocations. Besides, the empirical formulae expressing the tangential grinding force T are given as follows, where T and N in kg/cm², n in number per cm², and a in μ^2.

Annealed carbon steel with a wheel of A46N

$$\left.\begin{array}{ll} \text{Soybean oil:} & T = 0.21\,N + 1.56\,n\,(a)^{0.896} \times 10^{-3} \\ \text{Emulsion:} & T = 0.35\,N + 1.56\,n\,(a)^{0.896} \times 10^{-3} \\ \text{Dry:} & T = 0.73\,N + 1.56\,n\,(a)^{0.896} \times 10^{-3} \end{array}\right\} \quad (18)$$

Hardened high speed steel with a wheel of A46H

$$\left.\begin{array}{ll} \text{Soybean oil:} & T = 0.10\,N + 3.02\,n\,(a)^{0.927} \times 10^{-3} \\ \text{Emulsion:} & T = 0.16\,N + 3.02\,n\,(a)^{0.927} \times 10^{-3} \\ \text{Dry:} & T = 0.32\,N + 3.02\,n\,(a)^{0.927} \times 10^{-3} \end{array}\right\} \quad (19)$$

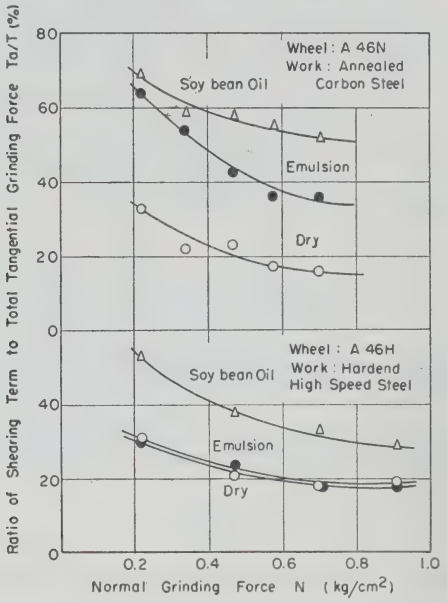

Fig. 15. Ratio of Shearing Term to Total Tangential Grinding Force.

Moreover, the rate of the shearing term in the total tangential grinding force may be calculated as shown in Fig. 15, and the following conclusions are given:

(1) In the case of annealed carbon steel, the rate of the shearing term with soybean oil is 50～70%. Compared with the value 20～30% in dry grinding, it suggests the remarkable antifriction effect.

(2) In the case of hardened high speed steel, the rate is 20～30% with dry grinding and emulsion. With soybean oil, it rises to 30～50%, but it is not so effective as in annealed carbon steel.

4. Principles of Cooling in Through Wheel Coolant Grinding[7]

In order to make clear the mechanism of cooling in through wheel coolant grinding, the temperature rise of the workpiece during grinding was measured by means of alumel-chromel thermocouple. As shown in Fig. 16 the thermocouple was

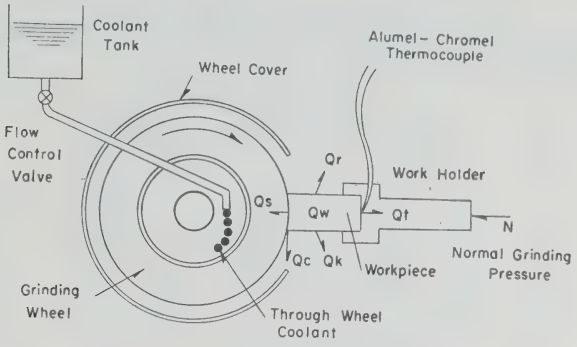

Fig. 16. Temperature Measurement and Heat Dissipation in Plunge-Cut Grinding

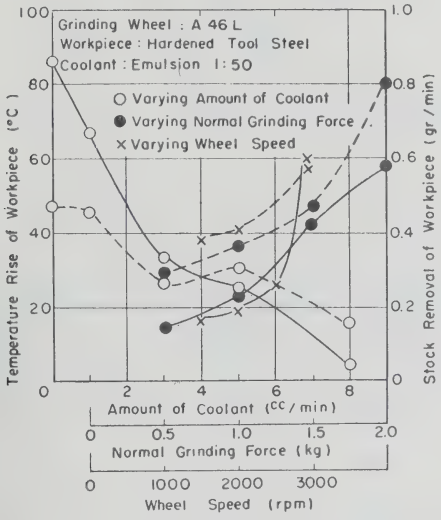

Fig. 17. Temperature Rise (full line) and Stock Removal (dotted line) in Through Wheel Coolant Grinding.

set between the workpiece and its holder, and the temperature rise after one minute grinding was measured, by varying the kinds and amounts of coolants, the grinding load, and the wheel speed.

One of the results with emulsion is illustrated in Fig. 17. This shows clearly that the amount of coolant is sufficient under 10 cc/min, and the temperature rise is approximately linear to the grinding load and the wheel speed. The stock removal of the workpiece is also plotted in dotted lines. Similar experiments were carried out with kerosene and soybean oil. Summarizing the data, the temperature rises under the standard conditions, where the grinding load was 1.0 kg, the wheel speed was 2000 rpm, the amount of coolant was 10cc/min, and the stock removal was 0.5 g, were calculated. The results are shown in Fig. 18, together with the grinding

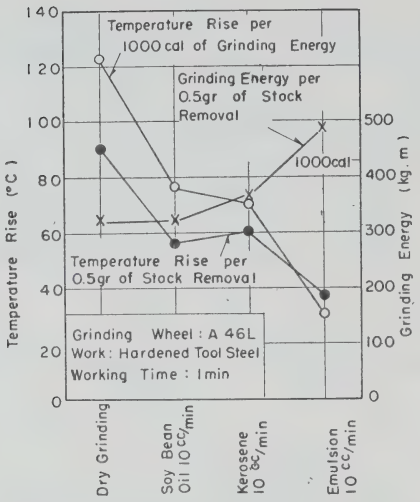

Fig. 18. Temperature Rise and Grinding Energy with Various Through Wheel Coolants.

energy per 0.5 g of the stock removal and the temperature rise per 1000 calories of the grinding energy.

Let the total heat generated in grinding be Q, and let us consider the heat balance as already described in Fig. 16. When the heat carried away with the chip is Q_c, the heat conducted to the wheel is Q_s, the radiated heat from the workpiece is Q_r, and the heat conducted to the workpiece holder is Q_t, then the rest consists of the heat remaining in the workpiece Q_w and the heat diminished by coolant Q_k. Then

$$Q = \{(Q_c + Q_s + Q_r) + Q_t\} + Q_w + Q_k . \tag{20}$$

From the previous study of the author[5], it is known that the ratios of the former three items to the total heat are 4%, 12% and 10% respectively. Assuming the ratio of Q_t to Q to be 15%, the equation may be rewritten as

$$(1 - 0.41)\, Q = Q_w + Q_k . \tag{21}$$

The remaining heat in the workpiece Q_w is also presumed to be calculated by

$$Q_w = \frac{\text{heat remaining in dry grinding}}{\text{temperature rise in dry grinding}} \times \text{temperature rise in through wheel coolant grinding}$$

Accordingly, the heat diminished by coolant Q_k can be determined numerically. The results are listed in Table 3 where the rate of stock removal is 0.5 g/min.

The values of Q_k in the last line of Table 3, are unexpectedly high. Because of a small amount of coolant used, it must be considered that the liquid may evaporate at the surface of the workpiece and the heat of evaporation may prevent

Table 3. Heat Diminished by Coolant Q_k

Coolant		Dry	Soybean oil	Kerosene	Emulsion
Temperature Rise of Workpiece	ΔT°C	92	55	60	35
Total Heat	Q cal	750	740	845	1140
Heat Carried Away	$0.41\,Q$ cal	308	304	346	467
Remained Heat	Q_w cal	442	264	288	168
Heat Diminished by Coolant	Q_k cal	/	172	211	515

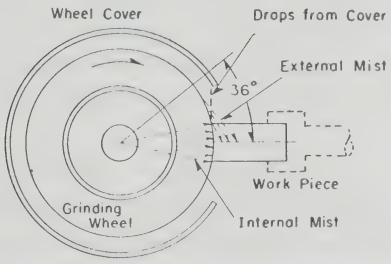

Fig. 19. Formation of Mist in Through Wheel Coolant Grinding.

Table 4. Cooling Calories in Through Wheel Coolant Grinding

Coolant	Soybean oil	Kerosene	Emulsion
Cooling Calories by Specific Heat in cal.	26	6	8
Cooling Calories by Evaporation in cal.	13	19	95
Total in cal.	39	25	73

the temperature rise. For a rough estimation of cooling calories, it is assumed that the temperature of the liquid poured directly to the workpiece rises up to its boiling point and the liquid evaporates perfectly. The ratio of internal mist to the total may be considered to be the ratio of the contact area of the work to the wheel periphery. It is roughly 0.024 as shown in Fig. 19. Then, the cooling calories in Table 4 may be calculated numerically.

However, these values are very small compared with the values of Q_k in Table 3. Even if these values in Table 4 multiply four-fold, assuming 10% of the total coolant may vaporize, the cooling calories have yet about half the values of Q_k in Table 3. This leads to a thought that the cooling effect by the liquid poured from the wheel cover may be considerable.

From the foregoing consideration and calculation, the principles of cooling in through wheel coolant grinding may be concluded as follows:

(1) It is fundamental that the coolant reaches the wheel-work contact surface in the form of mist, and then evaporates. The heat of evaporation seems to play a leading part in cooling effect.

(2) The mist of coolant sprayed upon the outside of the workpiece is considerably effective.

(3) Cooling effect by the liquid poured from the wheel cover is also important.

5. Conclusion

Through wheel coolant grinding is a novel method for lowering the grinding temperature and preventing the grinding burn. The tangential force in plunge-cut grinding with various coolants was measured by a newly designed bevel-gear torquemeter for through wheel coolant grinding. The temperature rise of the workpiece was measured by an alumel-chromel thermocouple.

From the experimental data and their analysis, the following conclusions were obtained:

(1) The coefficient of friction in grinding was determined. Soybean oil was the most effective of through wheel coolants, and coefficient of friction was 0.1 $\sim$0.2, which was about one third of that in the case of dry grinding.

(2) Analytical formulae representing the tangential grinding forces were derived from the specific shearing force in grinding. Then, the rate of the shearing term in the total tangential grinding force was calculated. With soybean oil, it was 50$\sim$70% in annealed carbon steel, and 30$\sim$50% in hardened high speed steel, while with dry grinding, it was only 20$\sim$30% in each case. This showed a remarkable antifriction effect of soybean oil.

(3) In through wheel coolant grinding, it was fundamental that the coolant reached the wheel-work contact surface in the form of mist and then evaporated. The heat of evaporation seemed to play a leading part in cooling effect.

Acknowledgement

The author wishes to express his appreciation to Mr. Kumazawa and Mr. H. Takahashi for their assistance in carrying out the experiments.

References

(1) Grit and Grinding, Vol. 45 No. 6 (1954).
(2) T. Sasaki and others: Trans. Japan Soc. Mech. Engrs., Vol. 21 No. 106 (1955) p. 427 (in Japanese).
(3) M. Ando and H. Inao: Mechanical Engineering (Japan), Vol. 2 No. 12 (Dec. 1954) p. 56 (in Japanese).
(4) G. Pahlitzch u. J Appun: VDI-Z., Bd. 96 Nr. 11/12 (1954) s. 320.
(5) K. Sato: J. of the Society for Precision Mechanics of Japan, Vol. 22, No. 4 (1956) p. 127 (in Japanese).
(6) K. Sato: J. of the Society for Precision Mechanics of Japan, Vol. 22 No. 12 (1956) p. 503 (in Japanese).
(7) K. Sato: Science of Machine, Vol. 7 No. 12 (1955) p. 1145 (in Japanese).

Criterion of Grinding Wheel Tool Life

Hiroyuki Yoshikawa
The Institute of Physical and Chemical Research, Bunkyo-ku, Tokyo

1. Introduction

Sharp edges of abrasive grains on a grinding wheel produced by dressing action undergo various changes during grinding operation in accordance with the nature of wear of the wheel. Gradual deterioration of grinding performance of a wheel is attributed to this process. At some extent of the deterioration, one must dress the wheel surface again to continue the right operation. The period between the two dressings is called the tool life of a grinding wheel. From the practical view point, establishment of the criterion of the tool life is very important.

The changing process of grain cutting edges has been directly observed by Peklenik[1], Schwarz[2] and Tsuwa[3] under microscope. They found that the plateau area easily grew at the top of cutting edges. Peklenik[1] suggested that the effect of plateau area on the grinding performance is similar to that of flank wear of a cutting tool on its cutting performance.

The purpose of the present paper is to describe the grinding performance of a grinding wheel in connection with its surface conditions. The grinding performance is expressed in terms of grinding force. The increase of plateau area is measured by an optical method. A criterion of tool life based on a characteristic curve of grinding force versus plateau area obtained by experiments is proposed.

2. Experimental

2.1 Procedure

A JUNG surface grinding machine was used. Work material was chromium-molybdenum steel, quenched and tempered. Grinding wheels used were of aluminium oxide, of #46 grit size and of 48% of grain. Their grades were varied by changing the amount of bond material in wheels. Diameter of the wheel was 225 mm with grinding width of 5 mm. No coolant was employed. Before an operation, wheel surface was dressed by a sharp diamond dresser with successive depths of cut of 0.02, 0.01 and 0.005 mm and with the feed of 1 mm/sec.

Grinding forces were measured by a strain-gauge type dynamometer with four strain rings. Between successive force measurements, griding was made on a test piece which was fixed directly on a magnet chuck to prevent the wheel wear from the effect of vibration which may occur from the low stiffness of the dynamometer.

Total plateau area on a wheel was measured optically by the method of Peklenik[1]. The white traces of the photograph were cut off and weighed. The ratio of the total weight of cut-off pieces to the weight of original photograph was taken as the area fraction of total plateau area on the wheel surface.

2.2 Results

Characteristic curves shown in Fig. 1 were obtained by the measurement of grinding forces. Curves in Fig. 1 represent the results on wheels of various grades. General characteristics derived from these experiments are summarized as follows:

1) Grinding force at the initial stage of grinding soon decreases.

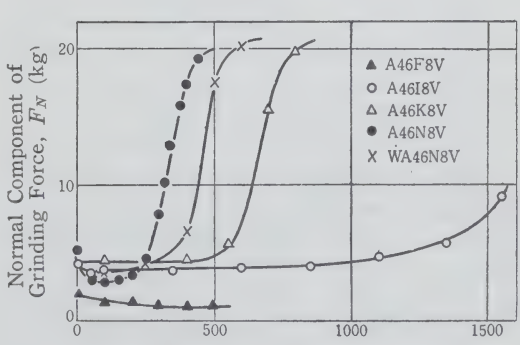

Fig. 1. Changes of grinding forces, with various wheels. Work: chrome-molybdenum steel, grinding condition: V=2000 m/mm, v=10 m/min, d=0.01 mm/st., width of work 5 mm.

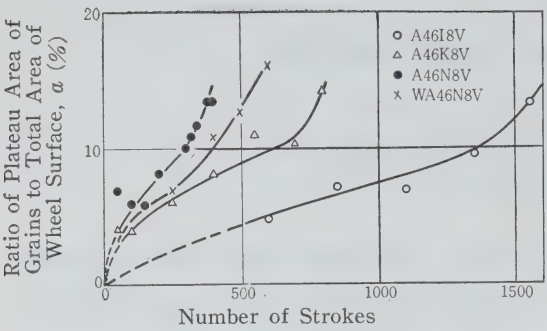

Fig. 2. Increase of plateau area in grinding. Grinding conditions are the same as specified in Fig. 1.

2) It remains almost constant for some time.

3) After remaining constant, the grinding force increases abruptly. This increase is 2∼3-fold for tangential component F_T and 7∼8-fold for normal component F_N except when the wheel is too low in grade or the grinding condition is too severe.

4) After reaching the highest value, the grinding force remains again constant for ever.

5) The increase of grinding force and the burn of ground surface occur at the same time.

Measurement of plateau area on the wheel surface by the aforementioned method was made in parallel with the measurement of grinding force. The results are shown in Fig. 2. which corresponds to Fig. 1. The ordinate is the ratio of total plateau area to total area of the grinding wheel. Abrasive grains on a grinding wheel surface, dressed afresh, are considered very complex in form. Most grains may have brittle-fractured in dressing process by a diamond dresser. Because of poor reflection from such grains, photographic method is of no avail to reveal the detail of wheel surface at the start of test. But soon after a little grinding, burnishing action of work material begins to give rise to specularly reflective plateau area on many favourably shaped grains as we see in rapid increase of plateau area in the initial stage of grinding shown in Fig. 2. In the second stage, progressing attritious wear and occasional fracture of cutting edges cause only a small increase of plateau area, which is shown by the gradual rise of the curves in the figure. In the third stage, the increase of area becomes large, this increase corresponds to the conspicuous rise of grinding force in Fig. 1.

3. Relation between grinding force and plateau area

In order to examine the relation between the grinding force and the plateau area of a grinding wheel, corresponding data are plotted in Figs. 3(a) and (b) as curves of normal and tangential components of grinding force respectively versus the percentage of plateau area. The simpleness of representation of data obtained on various kinds of wheel by a single curve is striking. Figs. 3 (a) and (b) reveal that both components of the grinding force remain constant before the percentage of plateau area reaches a critical value: 8% in this instance. Thereafter, they increase—the normal component F_N steeply, the tangential component F_T moderately. The fact that the data on different kinds of wheel lie on a single curve suggests that plateau area of cutting edges on wheel is the main factor that determines the grinding performance of a wheel.

From this characteristic curve, we obtain a criterion for the tool life of grinding wheel by the observation of wheel surface. This is very similar to the tool-life criterion of cutting tools. For example, when the grinding operation is required to be free from surface burn, the wheel should be dressed again before the plateau area exceeds 8%.

Strictly speaking, the curve of grinding force F versus percentage a of plateau area (hereafter called $a-F$ curve) differs by different grinding conditions: the lighter the grinding condition is set, the smaller becomes the critical value a_c of the area, which value is different for different kinds of work material. The effects of heat treatment of work material and coolant used in grinding on the value of a_c were also clarified. The detail of these investigations will be reported in near future.

4. Discussion

The fact that the grinding force F_N sharply increases when the plateau area exceeds 8% rather seems anomalous. If we think of an idealized case that every grain cutting edge gives the same depth of cut even when worn

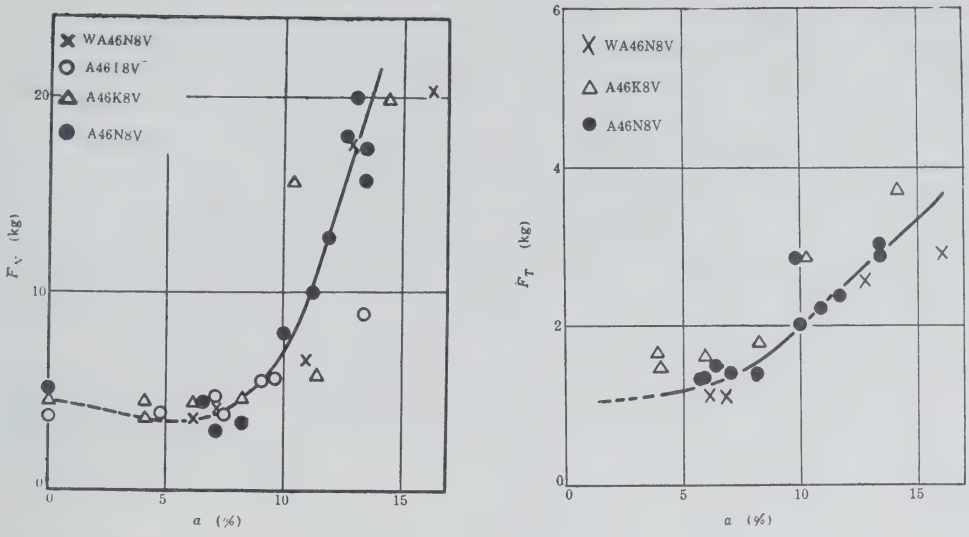

Fig. 3. (a) a-F curve (normal component), which shows the relation between grinding force and the ratio of plateau area of grains to total area of wheel surface. Data of Figs. 2 and 3 were used for the plot. (b) a-F curve. (tangential component)

with considerable plateau area, we can not expect such an anomaly, for the grinding force will increase only proportionally to the increase of plateau area.

In actual grinding action of a wheel, the assumption that every cutting edge gives the same depth of cut does not hold. A grain with plateau area requires some force to bite at and cut metal. Insufficient force will only cause elastic deformation of the metal or simply sliding.

A model experiment was made to ascertain this transition from sliding to cutting with a device. Conical diamond tools with flat area of various sizes were pushed onto a moving metal with gradual increase of load. The diamond tool was fixed to a load cell, with which the normal and tangential forces were detected. An example of oscillographic record of the forces is shown in Fig. 4. As the vertical feed of the tool was increased, the vertical as well as the horizontal, which is the frictional, forces increased linearly, but after a while, the latter underwent a rapid increase deviating from linearity, which showed a rapid increase of friction. Examination of the tool trace on the metal tells that it is no more than a polishing at first, but after the start of the

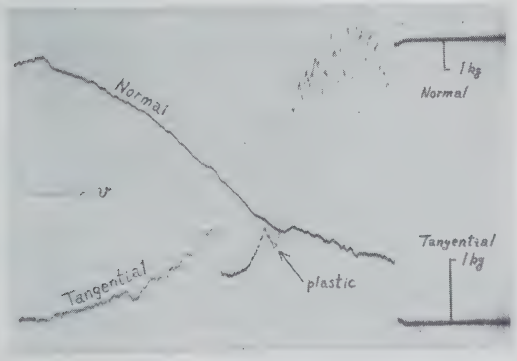

Fig. 4. Oscillogram of normal and tangential components of scratching force. At the point indicated by "plastic", cutting begins in the trace of scratching.

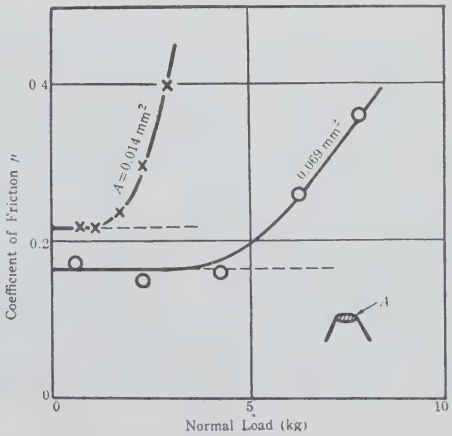

Fig. 5. Increase of coefficient of friction with increasing normal load.

rapid increase of friction, it is a plastic scratching, which is a sure indication of the transition from sliding to cutting. Curves of friction coefficient versus normal load are shown in Fig. 5. The above leads to a conclusion that a tool with a large flat area requires a large normal force to effect plastic scratching on metal. The normal stress on the contact area at the transition was found to be independent of the kind of tool, about 60 kg/mm^2 for the metal used.

Returning to the problem of grinding, we find that the plateau and stiffness of bond bridge are different from grain to grain. A grain with a large plateau area and bond bridge of low stiffness fails to acquire enough normal force to cut metal but simply slides in the state of elastic contact. A schematic illustration of such state is presented in Fig. 6. The contact area between wheel and metal is divided into two parts: one is

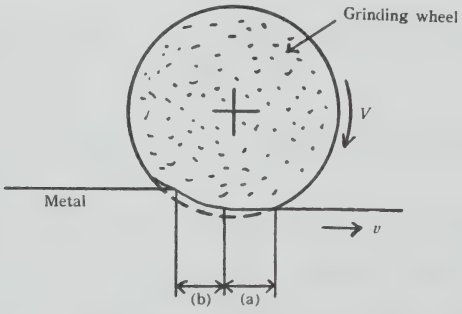

Fig. 6. Schematic illustration of grinding with large plateau area on the wheel. (a) Sliding part in which ineffective grains are engaged, (b) cutting part in which effective cutting edges are engaged.

the sliding part in the early stage of contact, in which the elastic deformation of the wheel is too small to produce enough grinding force, the other is the cutting part in the later stage of contact. In the sliding part, the force on cutting edge is for overcoming the friction, not for cutting. Hence, let such edge be called the ineffective edge, and when the number of grains with ineffective edge increases, it is only the grinding force that is increased. The experiment with the model showed that the friction coefficient increased from 0.2 to 0.5. This indicates that, before the plateau area reached 8% of the wheel surface, there were no ineffective grains, but after it passed 8% mark, there were fair number of ineffective grains, for, at this critical value of percentage, the ratio of tangential component of grinding force changes from 0.2 to 0.5. The fact that the rate of increase of plateau area became higher in the third stage of grinding as shown in Fig. 2 can probably be attributed to the increase of energy required for removal of every unit volume of metal.

Exact relation between the number of ineffective grains and the total plateau area can not yet be discussed for want of data. Further investigation is necessary.

5. Conclusion

It has been pointed out that the curve of grinding force versus the total plateau area, the $a-F$ curve, provides a criterion of tool life of grinding wheels. The shape of $a-F$ curve, however, is different for different work materials. When the grindability of work material is concerned, this $a-F$ curve may be an important factor for its evaluation. The grindability of a work material should be expressed in terms of the resistance against deterioration of wheel surface and also of the shape of $a-F$ curve.

In actual grinding operations, other criteria may sometimes be necessary: e.g., wheels, when too low in grade, tend to lose the right form and produce a poor surface finish, and hence the tool life of a grinding wheel should be determined by the degree of deviation from its original form. These criteria are now under investigation.

The author wishes to thank Prof. Makoto Okoshi for his suggesting the study on this problem and helpful discussions.

References

1) J. Peklenik: Untersuchungen über das Verschleisskriterium beim Schleifen, Industrie-Anzeiger, Vol. 80, No. 27 (1958) 397
2) K.Schwarz: Eine Filmeinrichtung zur Erffassung der Vorgange in Schleifscheibengefüge, Industrie-Anzeiger, Vol. 80, No. 92 (1958) 18
3) H. Tsuwa: On the Behaviors of Abrasive Grains in Grinding, I, Jour. Soc. Precision Mechanics, Japan, Vol. 26 (1960) 199

レジノイド砥石の研削液による劣化

花岡忠昭　木下直治*

Deterioration of Resinoid Grinding Wheels in Grinding Fluid.

by Tadaaki HANAOKA　Naoharu KINOSHITA

(別　刷)
千葉大学工学部研究報告　第14巻　第26号
1963年10月

UDC 621.92 : 620.16

レジノイド砥石の研削液による劣化

花岡忠昭　木下直治*

Deterioration of Resinoid Grinding Wheels in Grinding Fluid.

by Tadaaki HANAOKA　Naoharu KINOSHITA

レジノイド砥石はしばしば湿式研削に使われている．しかしレジノイドボンドはアルカリ性の研削液におかされやすい．したがってアルカリ性の研削液に長時間浸って研削作業が行われた場合，当然砥石が劣化するものと思われる．本研究は研削液のアルカリ度，浸漬時間，液温，濃度および砥石の組織を変えた場合のレジノイド砥石の劣化について実験を行った．この結果砥石の強度は浸漬条件によって大きく低下し，なかでも浸漬時間，液温，粒度による影響が大きい．一例をあげれば，粒度 80 の砥石を 0.1% のアルカリ溶液に一時間つけるとその強度は乾燥時の値の 50% に低下する．強度の低下は砥石の軟化を来し，砥石減耗を増大する．

Nomenclature

The following nomenclature is used in the paper:

W	weight of test bar before soaking (g)
W′	weight of test bar after soaking (g)
t	soaking time (hr)
C	liquid concentration (%)
T	liquid temperature (°C)
d	diameter of grain (μ)
Vb	bond percentage (%)
Gsp	bulk specific gravity
σ dry	bending strength of test bar before soaking (kg/mm²)
σ wet	bending strength of test bar after soaking (kg/mm²)
δ dry	deflection of test bar before soaking (mm)
δ wet	deflection of test bar after soaking (mm)
Pdry	scratch strength of test bar before soaking (kg/mm²)
Pwet	scratch strength of test bar after soaking (kg/mm²)

Introduction

In recent years resionid grinding wheels bonded with thermosetting resin (phenolic resin) are widely used for heavy grinding and fine grinding. However, phenolic resin is most susceptible to weakening action of the alkali solution, therefore, it

(受理　1963 年 7 月 13 日)　* 東洋大学

may be cosidered that the strength of the wheel is lost to a considerable extent if it is subjected to wet grinding for long time. This paper presents the results of deterioration of resinoid grinding wheels in grinding fluid at various soaking time, liquid temperature, liquid concentrations and structures of wheels.

Experimental works and results

Dissolution of the bond

The relation between liquid concentration and weight loss percent of test bar $(W-W'/W\times100)$ is shown in Fig. 1, which illustrates the results of soaking test of 80 grits bars of Vb=24%, Gsp=2.3 in NaOH solution for 1 hour. The horizontal axis of Fig. 1 is labelled with variable of the liquid concentration and the vertical with variable of weight loss percent of test bar. Black symbols in Fig. 1 indicate the result at T=50°C and open symbols at T=20°C.

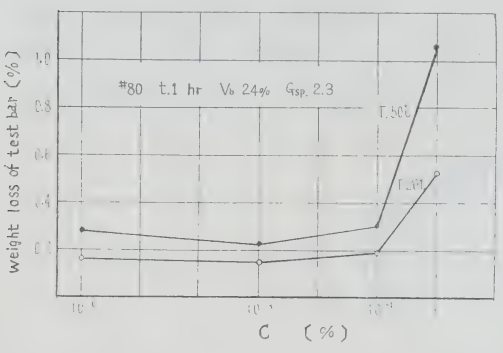

Fig. 1 Re ation between liquid concentration and weight loss percent of the test bar.

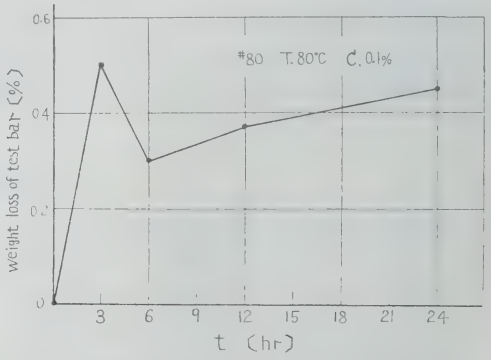

Fig. 2 Relation between soaking time and weight loss percent of the test bar.

As shown in Fig. 1, the weight loss is scarce until $C=10^{-1}\%$, but becomes rapidly remarkable beyond this value of concentration.

Relation between soaking time and weight loss percent of the test bar soaked into the liquid of C=0.1% at T=80°C is shown in Fig. 2. Weight of the test bar rapidly recreases in the initial stage of soaking, but the decrease is pretty slow afterwards. This characteristic inclination of the decrease will be due to reduction of surface area of the bond, for solubility of the bond in unit time is proportionate to its surface area.

Influence of soaking time

80 grits test bars were subjected to soaking (at T=80°C) of various soaking time, 1 hour, 3 hours, 6 hours, 12 hours and 24 hours, and the resulted change in strength and the deflection of the test bars were observed.

In the horizontal axis of Fig. 3 is plotted the variable of the soaking time and in the vertical axis, variable of the ratio σ wet/σ dry. The relation between the ratio

σ wet/σ dry and soaking time is shown with black symbols in the figure. This curve shows a sharp line until 6 hours and then a mild slope afterwards. This curve on the logarithmic graph is linear, therefore the relation between t and σ wet/σ dry is represented as follows

$$\sigma \text{ wet}/\sigma \text{ dry} = 0.5\, t^{-0.24}$$

The exponent here changes depending upon the soaking condition. As indicated by the open symbols in the figure, there is a definite relation between soaking time and δ wet/δ dry that δ wet/δ dry increases with soaking time.

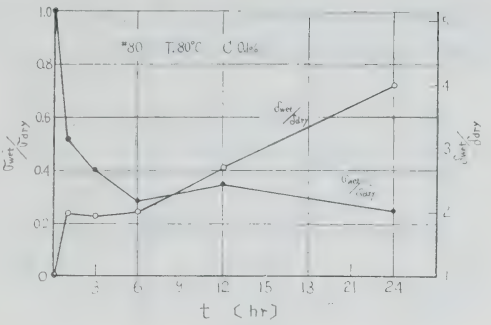

Fig. 3 Relation between soaking time and σ wet/σ dry, δ wet/δ dry.

It may be considered that the loss of the bending strength in the test bars is due to dissolution and softening of the bond.

Influence of liquid concentration

After 80 grits test bars were soaked for 24 hours in liquid (at T=80°C) of various concentrations, 10^{-6}%, 10^{-3}% and 10^{-1}%. The strength of the test bar was measured respectively. The result is shown in Fig. 4 in the logarithmic graph. Because of the linearity of the curve in the figure, the relation between C and σ wet/σ dry is represented as follows

$$\sigma \text{ wet}/\sigma \text{ dry} = 0.36\, C^{-0.04}$$

δ wet/δ dry increases slightly with rise in the liquid concentration. As shown in Fig. 2, the bond does not dissolve in the liquid concentration under 0.1%, and also the bending strength of the bond does not get lost in the liquid concentration under 0.1% as shown in Fig. 4.

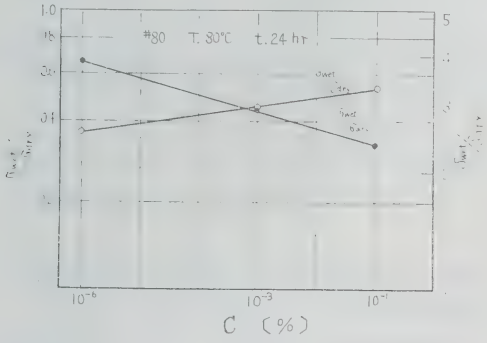

Fig. 4 Relation between liquid concentration and σ wet/σ dry, δ wet/δ dry.

Influence of liquid temperature

80 grits test bars were subjected to 24 hours soaking in the liquid (C=0.1%) of various liquid temperatures, 20°C, 40°C, 60°C and 80°C, and the strength of the test bars was tested afterward.

The horizontal axis of Fig. 5 is labelled with variable of the liquid temperature and vertical axis with variable of the ratio σ wet/σ dry. The relation between the ratio σ wet/σ dry and liquid temperature is plotted with black symbols. The ratio

σ wet /σ dry decreases with the rise of the liquid temperature, while the ratio δ wet /δ dry increases rapidly with T.

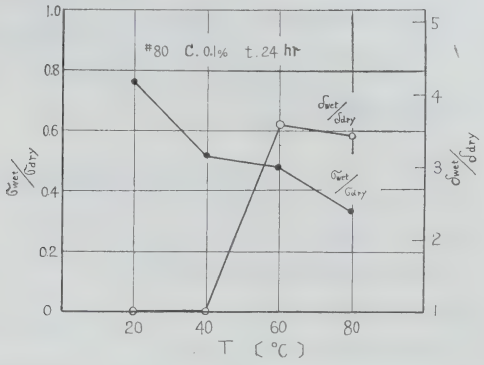

Fig. 5 Relation between liquid temperature and σ wet/σ dry, δ wet/δ dry.

The strength of the resin used as the bond material is not lost at the temperature under 200°C. Otherwise, as shown in Fig. 5 the loss of bond strength at higher liquid temperatures may probably be explained by the increase of permeability of the liquid and softening of the bond through elevated temperature.

Influence of grain size

The relations of grain size with σ wet/σ dry and with δ wet/δ dry are shown in Fig. 6 respectively, in which is plotted the results of a soaking test performed on test bars (Vb=24%, Gsp=2.3) of various grain sizes 16, 36, 60 and 80, for 24 hours in the 0.1% liquid concentration. The relation between d and σ wet/σ dry is plotted with black symbols. The curve thus obtained is linear, and the similar relation is also found between d and δ wet/δ dry.

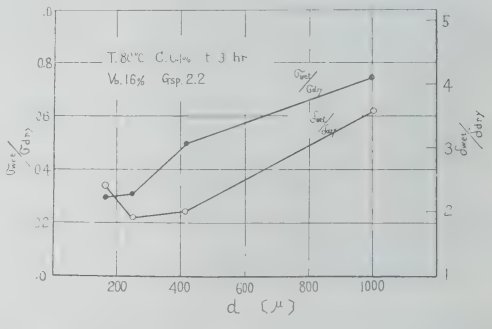

Fig. 6 Relation between diameter of grain and σ wet/σ dry, δ wet/δ dry.

Influence of structure of wheel

After 60 grits test bars (Gsp=2.2) of various bond percent, 8%, 12%, 16%, 20% were soaked for 3 hours in the liquid (C=0.1%, T=80°C), the strength of test bars was tested after soaking.

The relation between bond percent bending strength is shown in Fig. 7. The signs x in the figure indicates the values in dry state, and the black symbols those in wet condition. Bending strength of the test bars increases in proportion to the rise of bond percent in the test bars in both conditions.

As shown in Fig. 8 the ratios, σ wet/σ dry, δ wet/δ dry, does not vary regardless of increase of bond percent of the test bar.

Next a relation between bulk specific gravity and bending strength is studied by using 60 grits test bars of Vb 16%. Test bars of different Gsp 2.0, 2.3, and 2.6, were dipped in the liquid of C=0.1% at T=80°C. The relation found in the test is plotted in Fig. 9, and relations of the bulk specific gravity with σ wet/σ dry and with δ wet/δ dry respectively are shown in Fig. 10. The ratio σ wet/σ dry in-

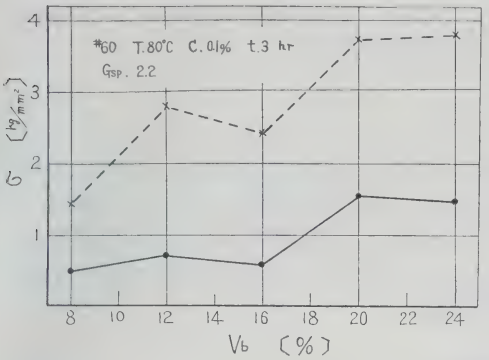

Fig. 7 Relation between bond percent and bendind strength.

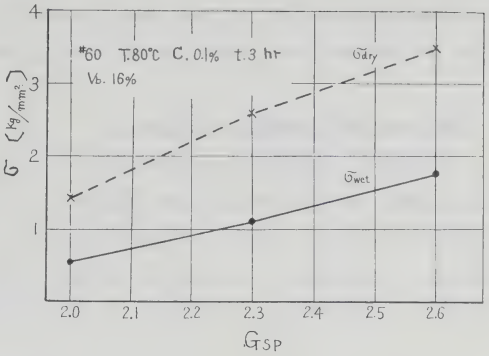

Fig. 9 Relation between bulk spesific gravity and bendind strength.

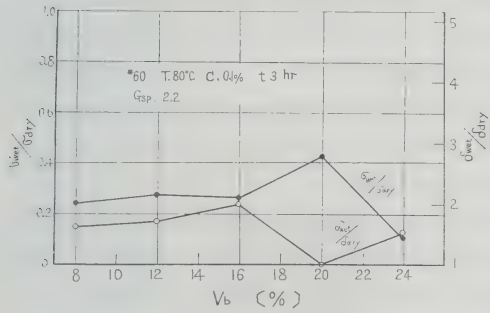

Fig. 8 Relation between bond percent and σ wet/σ dry, δ wet/δ dry.

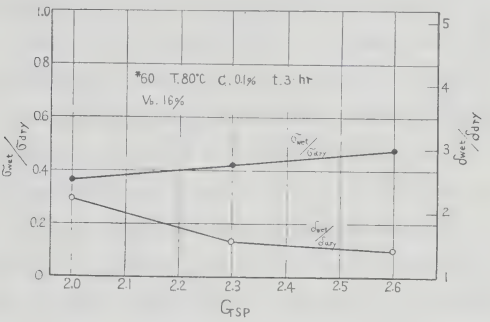

Fig. 10 Relation between bulk specific gravity and σ wet/σ dry, δ wet/δ dry.

creases slightly with bulk specific gravity, while on the other hand δ wet/δ dry decreases.

Decrease in grade of wheel

The scratch strength of the test bars used in the above soaking experiment was measured by the OKOSHI's grade tester. It was thus found out that the loss of scratch strength of the specimens by soaking in the liquid is quite similar to their loss in bending strength.

The relation between Pwet and σ wet is shown in Fig. 11, and the following can be obtained from the figure.

$$P\,\text{wet} = 7\sigma\,\text{wet}$$

and the value of the ratio P wet/P dry

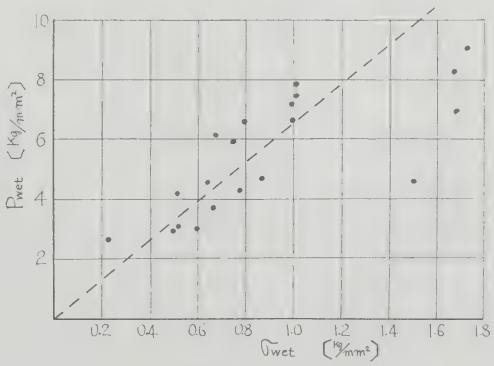

Fig. 11 Relation between bendind strength and scratch strength.

is the same as that of the ratio σ wet/σ dry. Thus, it will be possible to replace the abovementioned relation of σ wet/σ dry with P wet/P dry.

Decrease of grinding efficiency

When the bending strength of the wheel is lost and the grade of the wheel decreased, it may be evident that the wear of the wheel becomes great. Then, as shown in Fig. 3, the bending strength of the wheel, if soaked in the liquid for 1 hour, is reduced to a half of its strength in dry state, hence the wear of the wheel in wet is less than one-fourth of its wear in dry.

Conclusion

An investigation was made on deterioration of resinoid wheels in grinding fluid at various soaking time, liquid temperatures, liquid concentrations and structures of the wheel. As the result, it became evident that the loss of the strength in the wheel in different in response to change of soaking condition. The most influential among other conditions, are soaking time, liquid temperature and grain size.

It may be remarked that the strength of the wheel is more reduced by swelling of bond of the wheel than its dissolving into the liquid.

For an example, the strength of the wheel was reduced to 50% of its dry value when 80 grits wheel was soaked in 0.1% alkai solution for 1 hour at 80°C. The grinding efficiency is decreased greatly by the loss of the strength of wheel.

The authors acknowledge their indebtedness to Dr. Kumagai, the chairman of the J. S. G. E., for his helpful advice and suggestion.

(Received July 13, 1963)

ОТДЕЛОЧНОЕ ШЛИФОВАНИЕ ЗЕРКАЛЬНО ЧИСТОЙ ПОВЕРХНОСТИ САМОЗАТАЧИВАНИЕМ КРУГА

(СТИХИЙНЫМ ОБРАЗОВАНИЕМ РЕЖУЩИХ КРОМОК АБРАЗИВНЫХ ЗЕРЕН)

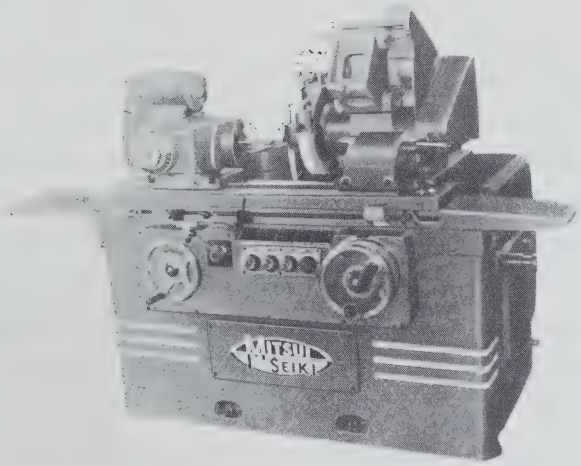

УНИВЕРСАЛЬНЫМ ШЛИФОВАЛЬНЫМ СТАНКОМ
ТИПА MUG 25–50

"Мицуи–Сэйки–Когио Ко. Лтд."
Ямато Шузо
Иокогава Казухико

ОТДЕЛОЧНОЕ ШЛИФОВАНИЕ ЗЕРКАЛЬНО ЧИСТОЙ ПОВЕРХНОСТИ САМОЗАТАЧИВАНИЕМ КРУГА (СТИХИЙНЫМ ОБРАЗОВАНИЕМ РЕЖУЩИХ КРОМОК АБРАЗИВНЫХ ЗЕРЕН)

"Мицуи—Сэйки—Когио Ко. Лтд."
Ямато Шузо
Иокогава Казухико

До Второй мировой войны, для получения зеркально чистой поверхности абразивом применялись станки суперфиниширования или полирования. После войны получил распространение метод получения зеркально чистой поверхности шлифованием. Фирма"Фритз Студер"разработала т. н. гибкие шлифовальные круги, которые состоят из зерен мельчайшей зернистости, удерживающихся бакелитовой связкой или резиной. В первое время отделочного шлифования зеркально чистой поверхности снимали этими кругами последний слой 0,002 мм по диаметру.

Вслед за этим, фирмой "Мицуи-Сэйки" изготовлены остекленные шлифовальные круги общего назначения марки WA 60JmV. Второй период отделочного шлифоания зеркально чистой поверхности характеризовался применением этих шлиховальны кругов. Задавая малую скорость для правки круга иолучали равномерные режущие кромки гранями абразивного зерна, затем, используя принцип "резца Геера" снимали последний припуск, 0,01 мм по диаметру в целях полученйя зеркально чистой поверхности.

Вскоре после этого, начался третий период отделочного шлифования зеркально чисой поверхности самозатачивающимся кругом. Этим методом не только снимали припуск 0,2 мм по диаметру, то-есть от черновой обработки и до получения зеркально чистой поверхности, но и за одну правку обрабатывали несколько деталей до зеркально чистой поверхности.

Ниже дается историческое описание исследовательских работ в этой области.

1. Отделочное шлифование зеркально чистой поверхности во второй период

Десять лет назад мы только еще производили опытно-экспериментные работы для получения зеркально чистой поверхности с помощью остекленного шлифовального круга общего назначения.

1.1 Отделочное шлиФование зеркально чистой повесхности в первыи мериод

В то време говорили, что чем мельче зернистость или выше твердость, тем лучше чистота шли-

фуемых поверхностей.

1.1.1 Зависимость шероховатости шлифуемых поверхностей от зернистости абразива.

расстояние между зернами на поверхности абразива зернистостью 46 составляет примерно 0,6 мм, а 60–6,4 мм, 80–0,3 мм. Размер зерна зернистстью 46 около 0,5 мм, а 60–0,33 мм, 80–0,25 мм. Сравнение зерен разной зернистостью, из котоых состсят поверхности шлифовальных кругов показано на **Фиг. 1.**

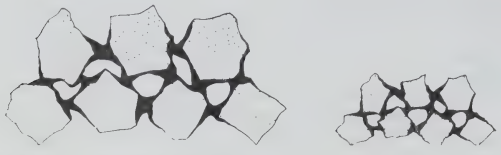

Зерно зернистостью 46 Зерно зернистостью 80

Фиг. 1 Сравнение зернистости зерен на поверхности круга (в одном масштабе)

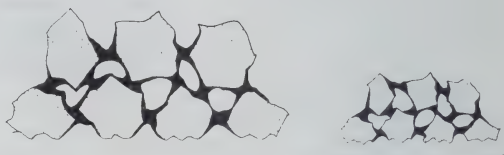

Зерно Зернистостью 46 Зерно Зернистостью 80

Фиг. 2 Зернистость Зерен на поверхности круга после черновой правки

На современном шлифовальном станке можено получишь скорость движения стола 1 мм/мин, однако, десять лет назад на шлифовальном станке минимальная скорость стола равнялась 100 мм/мин, и движение медленнее получить не удавалось. Поэтму, на шлифовальном станке получили 0,1 мм на один оборот шлифовального круга при наилучших режимах шлифования. Состояние зерен после праки показано на **Фиг. 2,** из чего видно, что грани зерен неравномерны и имеется множество неровностей. Отсюда ясно, что в то время, для обрабатываемой детали считали лучше применять шлифовальные круги с малым расстоянием между зернами, т. е. мельчайшей зернистостью.

В то время, само собою разумеетея не ставилась задача получить зеркально чистую поверхность. а производилось обычное шлифование. На **графике 3** показана зависимость чистоты шлифованной поверхности от замены абразивного зерна зернистостью 36–80. Приведенные данные взяты из прошлых экспериментов, и не основываются на опытно-экспериментальных работах с использованием современных шлифовальных станков, полученная чистота поверхности некачественна, но все же видно, что чистота шлифуемой поверхности зависит от величины зерна абразива.

Шлифовальный круг

WA-зернистость-K

Обрабатываемая деталь

S45C твердостью по Роквеллу 40

Окружная скорость шлифовального круга

30 м/сек

Окружная скорость обрабатываемой детали

21 м/мин

Подача для правки на один оборот шлифовального круга 0,15 мм/об

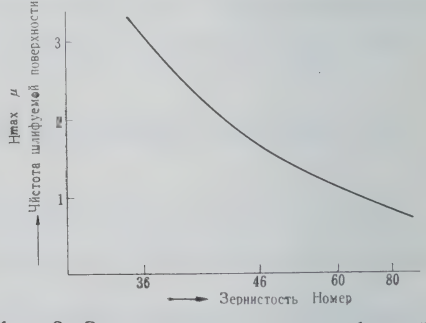

фиг. 3 Зависимость чистоты шлифуемой поверхности от Зернистости

Врезная подача алмаза правки	0,01 мм по диаметру
Врезная подача шлифовального круга	0,01 мм по диаметру
Количесвто проходов через одну шлифовальную точку	3
Количество ироходов Выхаживания	полудвойной ход

1.1.2 Завимоть чистоты шлиФуемой поверхности от твердсти щлиФовального круга

При повышенной твердости, зерна крепко удерживаются связующим веществом, поэтому рии производение правки в одинаковых условиях легко получить желаемые грани абрзивных для шлифования (**см. Фиг. 4. а**), безразрывов и выпадений зерен как это показано на (**Фиг. 4. в**), благодаря чему получается хорошая чистота поверхности. Однако, по мере повышения твердости зерен обнаруживаются недостатки, т. е. прижоги при шлифовании или шлифовочные трещины, так как при этол отсутствует самозатачиание круга с дальнейшим дроблением зерен н в процессе шлифования.

Фиг. 4 Выпадение и дробление зерен на поверхности Круга

1.2 Отделочное шлифование зеркально чистой поверхности во второй период

Всем известно, что применение "резца Геера"при точении и строгании позволяет легко получить равномерную поверхность. Отсюда ясно, что и при шлифовании с применением круга, на поверхности которого равномерны грани зерен, обеспечивается качественная чистота шлифуемой поверхности обрабатываемой детали. Иначе говоря, ири отсутствие осевого биения и вибрации шлифовального шпинделя,и возможности получить равномерную поверхность граней зерен абразива на шлифовальном круге (**см. Фиг. 5**), можно было бы сказать гтопочти половина задачи выполнена. Таким образом задача на второй период заключалась в создании равномерных граней зерен и их сохранении.

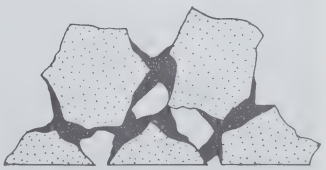

Фиг. 5 Гладко заправленные зерна на поверхности круга

1.2.1 Зависомость состаяния поверхностных зерен шлиФовального круга от скорости правки

На металлографии правки 1 показана грань с наибольшей шириной, полученная ири правке с подачей алмаза 0,05 м на один оборот круга. При правке с подачей алмаза 0,001 мм на один оборот круга получаетая множество широких граней зерен (**см. микрограф 2**). Значит, эксперименты показывают, что количество шлифуемых граней зерен и рабочая поверхность значительно колеблется в зависимости от скорости правки, следовательно при правке с малой скоростью, например с подачей алмаза 0,001 мм на один оборот шлифовального круга получаются равномерные режущие кромки, соответствующие лезвиям "резца Геера".

После шлифования заготовки этими запрявленными шлифовальными кругами рассмотрели поверхностные абразивные зерна с наибольшей шириной. Сравнение граней поверхностных абразивных зерен, начерно шлифованных при большой скорости правки (**см. микрограФ 3**), с гранями на **микрографе 4** показывает, что при малой скорости правки и чистом шлифовании получается множество граней, соответствующих режущим кромкам "реца Геера"

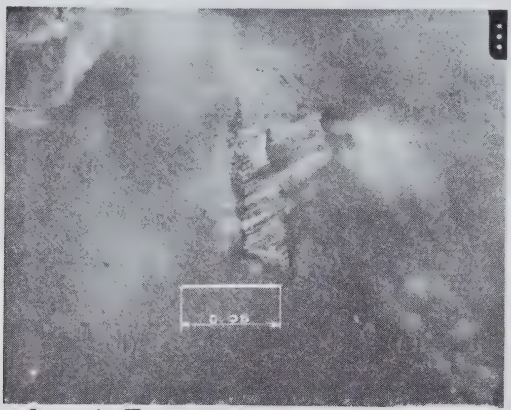

Фото. 1 Поверхностные зерна круга после правки (Подача алмаза 0,05 мм/об)

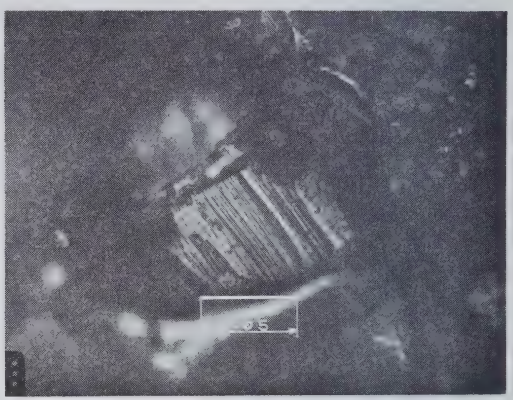

Фото. 2 Поверхностные круга после правки (Подача алмаза 0,001 мм/об)

1.2.2 Зависимость чистоты шлиФуемой поверхности от скорости правки

На **Фиг. 6** показано изменение шлифуемых поверхностей при врезной подаче с разными скоростями правки. При этом режимы шлифования следующие:

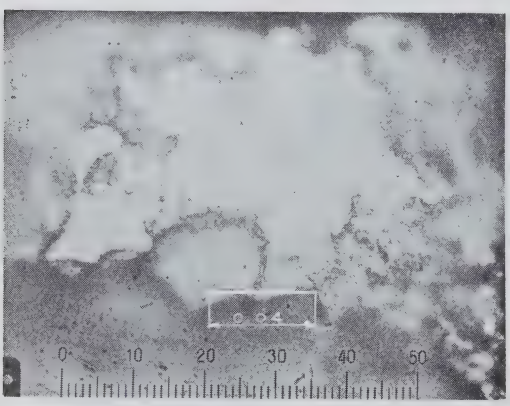

Фото. 3 Поверхностные абразивные зерна круга после шлифования (Подача алмаза 0,066 мм/об)

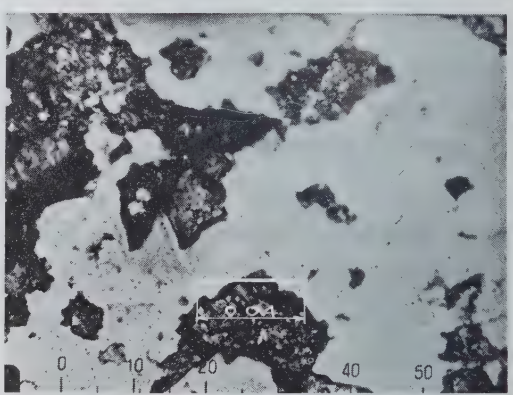

Фото. 4 Поверхные зерна круга после шлифования (Подача алмаза 0.002мм/об.)

Шлифовальный круг	WA 60JmV
Обрабатываемая деталь	S 45 C твердостью по Роквеллу 42
Сечение припуска на шлифование	3 мм^2
Окружная скорость шлифовального круга	33 м/сек
Окружная скорость обрабатываемой детали	10 м/мин

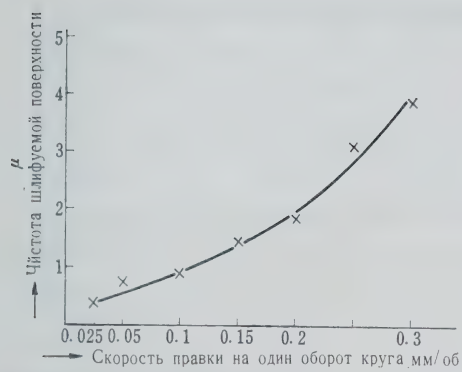

Фиг. 6 Зависимость чистоты шлифуемой поверхности от скорости правки

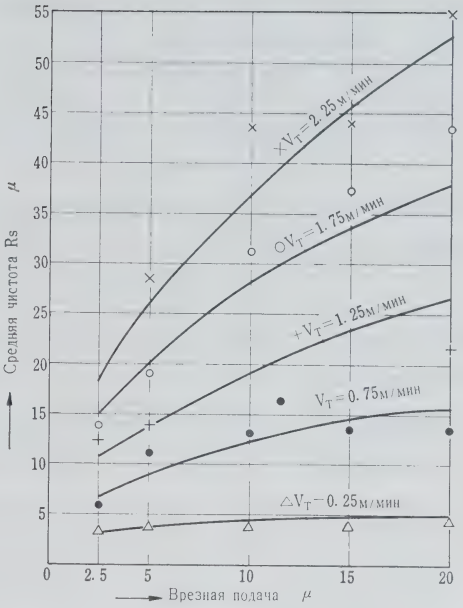

фиг. 7 Зависимость чистоты поверхности от врезной подачи алмаза правки (THÖING, W)

Врезная подача алмаза 0,002 мм по диаметру

Врезная подача шлифовального круга на один оборот обрабатываемой детали 0,002 мм по диаметру

Количество оборотов выхаживания 5

Из рисунка видно, что при меньшей скорости правки получаются равномерные грани зерен как показаны на микрографе 2 по параграфу

1. 2. 1 и создается более чистая поверхность шлиФования.

1. 2. 3 Зависимость чистоты шлиФуемых поверхностей от врезной подачи при правке

Когда задается большая подача алмаза при правке, то создается большая сила сопротивления, воздействующая на поверхностные зерна круга, что приводит к разрыву зерен или в крайнем случае к их выпадению. В результате чего образуются неравномерные грани поверхностных зерен, и получается большая неровность. Опыты показывают, что увеличение врезной подачи алмаза ухудшает чистоту шлифуемых поверхностей, при этом зависимость чистоты шлифуемых поверхностей от врезной подачи алмаза приве дена **на Фиг. 7,**

Для того, чтобы получить равномерные грани поверхностных зерен абразива считается производительным производить правку : два раза врезанием алмаза с подачей не более 0,005 мм по диамет - ру для чистового шлифования, и затем выхапеиванием получить равномерномерную поверхностть круга без влезания.

1. 2. 4 Соотношение чистоты шлиФуемой поверхности и Формы алмаза

В большинстве случаев применяются шарошки для правки однокаменным алмазом(**см. Фиг.** 8,**а**), И шарошек из алмазных порошков/200 меш/ (**см. Фиг.** 8,**в**) которые обеспечивают получение без

затруднения гладких граней поверхностных зерен абразива при большой скорости правки.

Виды алмазов	Однокаменный алмаз	Спеченный порошковый алмаз
Скорость правки	0, 02 мм/об	0, 035 мм/об
Чистота шлифуемой поверхности	0, 2 S	0, 1 S

Таблица 1 Виды алмазов, скорость правки и чистота шлифуемой поверхности

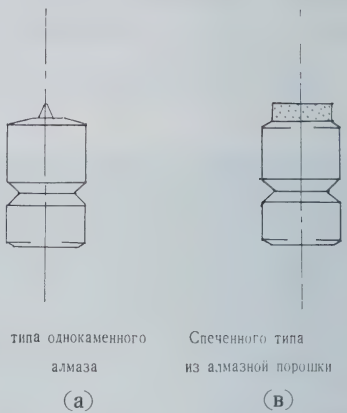

Фиг. 8 Виды шарошек для правки

В **таблице 1** приведены данные о чистоте поверхности шлифования зерен врезной подачей при применении различных алмазов и скоростей правки. При этом режимы шлифования следующие :

Шлифовальный круг	WA 46 JmV
обрабатываемая деталь	S 45 C твердостью по Роквеллу 42
Сечение припуска на шлифование	0, 75 мм^2
Окружная скороть обрабатываемой детали	7, 5 м/мин
Врезная подача алмаза правки	0, 005 по диамету

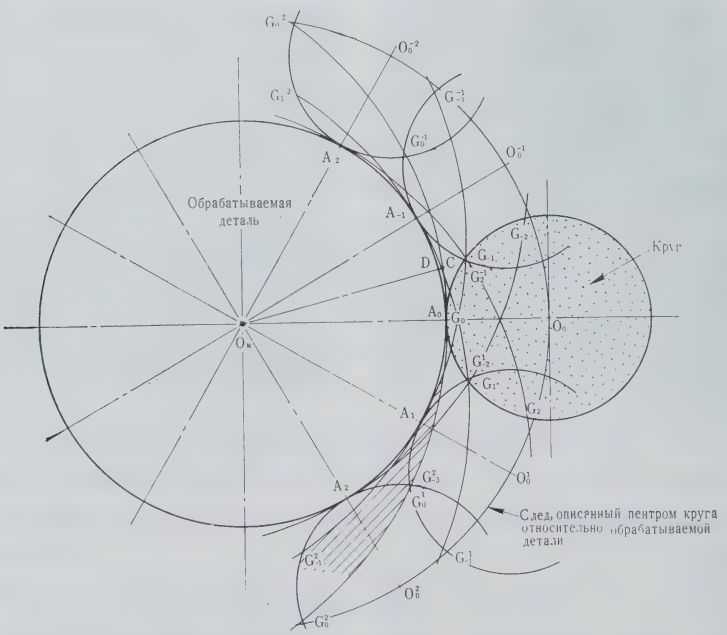

Фиг. 9 Модель шлифования для следов зерен и оставшегося припуска

Врезная подача шлифовального круга на один оборот обрабатываемой детали	0,2 мм/об по диаметру
Количество оборотов выхаживания	50

1.2.5 Соотношение чистоты шлифуемой поверхности и окружной скорости обрабатываемой детали

При присутствии беззазорных поверхностных зерен круга (см. **Фиг. 9**) обрабатываемая деталь шлифуется кривой G-2, G0, G2, соответствующей контуру круга, а при одном обороте обрабатываемой детали, последняя шлифуется по совершенной овальности, радиусом которй является Ow Ao от центра Ow. Однако, как изложено выше в параграфе 1.1.1 / зависимость чистоты шлифуемой поверхности от зернистости круга/, фактически между поверхностными зернами круга имеется определенное расстояние. Например, на поверхности круга, они распределяются по кривой G_{-2}, G_{-1}, G_0, G_1 и G_2. Теперь, если обрабатываемая деталь и шлифовальный круг приводятся во вращение с точки где расположено зерно G_0 на центровой линии от центра обрабатываемой детали Ow до центра шлифовального круга O_0, и центр шлифовального круга перемешается на положение O_0', а зерно G_{-1} перемещается на положение A_1 на центровой линии от центра O_0, соответственно смещаются зерно G_0 на положение G_0', G_1 на G_1', G_{-2} на G_{-2}'. Подобно этому, допустим положение зерна G_{-2} перешел на положение A2, то G_{-1} должно быть смещено на положение зерна G_{-1}^2, а G_0 на G_0^2, G_1 на G_1^2 и т. д.

По этой модели шлифования следы зерна G_1 образуют кривую G_1^{-2}, A-1, G_1 и G_1', следы верна G_0 образуют кривую G_0^{-2}, G_0^{-1}, A_0, G_0' и G_0^2, следы G-1 образуют кривую G_{-1}^{-1}, G_{-1}, A-1 и G_{-1}^2. Таким образом, оставшийся припуск при шлифовании зернами G_1 и G_0 составляет площаюь A-1, C и A_0, а CD будет шероховатостью. Следы зерна G_0- кривая A_0, G_0' и G_0^2 и следы зерна G_{-1}- кривая G_{-1}, A1 и G_{-1}^2 проходят наклонными линиями через площадь, которая представляет собою шлифуемую часть обрабатываемой детали зерном G_{-1}. Не трудно представить себе, что между A_0 и A1 тоже возникается поверхностная шерохватость оставшегося припуска подобно тому же как при CD.

Из фигуры следует, что при уменьшении окружной скорости обрабатываемого изделия расстояние между A-1, A0, A0, A1 должно укорочиться, следовательно чистота поверхности CD ухудшается. В обратном случае, если окружнан скорость шлифовального круга увеличится, то получится подобный же результат. Однако, прочность остекленного шлифовального круга для общего назначения не позволяет увеличивать окружную скорость больше 30 м/сек, поэтому как правило уменьшая окружную скорость обрабатываемой детали улучшают чистоту поверхности.

На **Фиг. 10** показана зависимость чистоты поверхности от окружной скорости обрабатываемой детали.

Шлифовальный круг	WA 46 LmV
Обрабатываемая деталь	S 45 C твердостьы по Роквеллу 24-26
Сечение припуска на шлифование	1850 мм^2

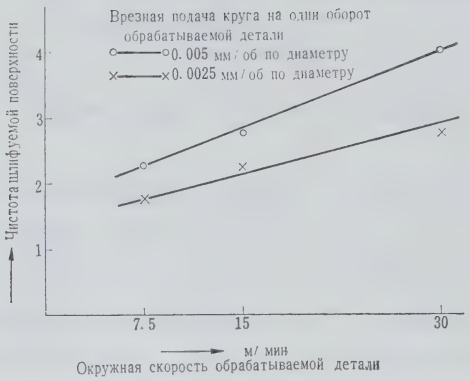

Фиг. 10 Зависимость чистоты шлифуемой поверхности от окружной скорости обрабатываемой детали

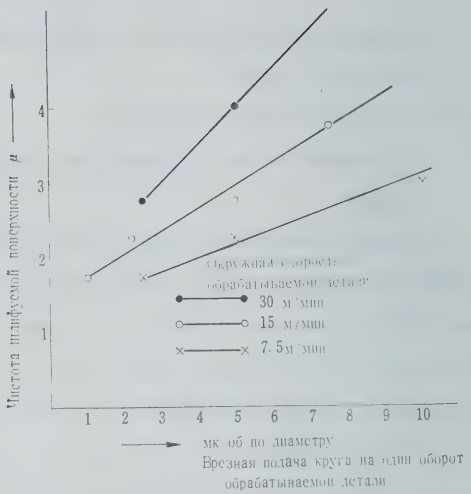

Фиг. 11 Зависимоть чистоты шлифуемой Поверхности от врезной подачи круга

Подача для правки на один оборот круга	0, 073 мм/об
Врезная подача алмаза правки	0, 01 мм по диаметру
Количество оборотов выхаживания	5

Эти эксперименты производились не для получения зеркально чистую поверхность, а лишь для снятия сечения припуска на шлифование, соответствующее полной производительности шлифовального круга. Экспериментами доказано, что чистота шлифуемой поверхности улучшается при уменьшении окружной скорости обрабатываемой детали.

1. 2. 6 Зависимость чистоты шлифуемой поверхности от врезной подачи шлифовального круга

Увеличение врезной подачи шлифовального круга вызывает разрыв поверхностных зерен круга в процессе шлифования, следовательно образуются неравномерные поверхности, что не обеспечивает качественную поверхность. На Фиг. 11 показана зависимость чистоты шлифуемой поверхности от врезной подачи шлифовального круга. Из кривых видно, что чем меньше врезная подача шлифовального круга, тем качественнее чистота шлифуемой поверхноти.

Режимы шлифования подобно тому как по паратграфу 1, 2. 5.

1. 2. 7 Зависимость чистоты шлифуемой поверхности от количества проходов через одну обрабатываемой детали

Как изложено в параграфе 1. 1. 1, плсщадь, занимаемая зернами в поверхности круга весьма мала, так как присутствует большое пространство между зернами. Таким образом, при определениой подаче круга по радиальному направлению, Все же обрабатывемая деталь не шлифуется равномерно, а остается определенный припуск. Поэтому, скорость стола уменьшается так, чтобы обрабатываемая деталь была отшлифована полностью наивысшими гранями зерен круга и, чтобы круг проходил несколько раз за одну и ту же точку обрабатываемой детали.

1.2.8 Результаты отделочного шлифования зеркально чистой поверхности во второй период

На фотографии 5 показано состояние отражающей поверхности обрабатываемой детали, отшлифованной с соблюдением условий отделочного шлифования зеркально чистой поверхности. На **Фиг. 12** показана чистота поверхности, которую определили "тэйлисэрфом" /профилометр с ощупывающей головкой датчиком/. При этом режимы шлифования следующие:

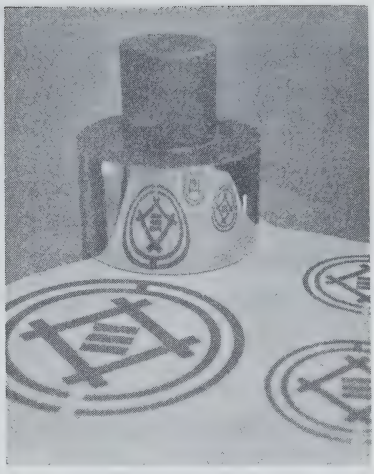

Фото 5 Отшлифованная зеркально чистая поверхность

Шлифовальный круг	WA 46 KmV
Обрабатываемая деталь	S 45 C твердостью по Роквеллу 45
Окружная скорость шлифовального круга	30 м/сек
Окружная скорость обрабатываемой детали	6 м/мин
Подача правки на один оборот круга	0,003 мм/об
Врезная подача алмаза правки	0,005 мм/по диаметру/
Врезная подача шлифовального круга	0,005 мм/по диаметру/
Количество проходов через одну точку шлифования	40
Выхаживание	полудвойной ход

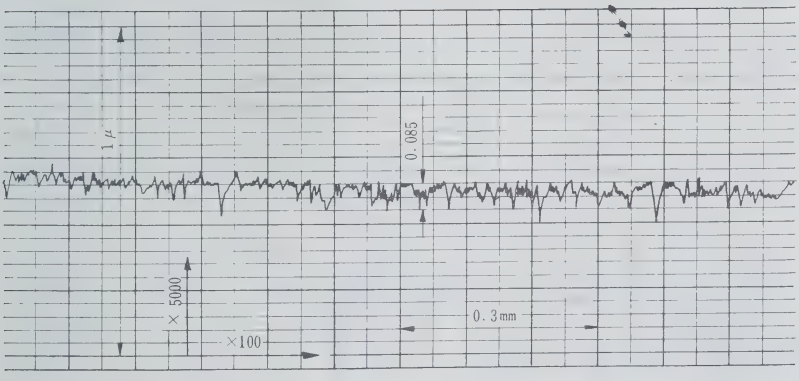

Фиг. 12 Чистота шлифованной поверхности

2. Соотношение самазатачиваний круга и режимов шлифования

Года три назад возникли многие непонятные вопросы, без решения которых невозможно понять подробности состояниями зерен в процессе шлифования. Выкрашивание и отделение зерен от поверхности круга в процессе шлифования, вот что было для нас проблеммой. Минуя эту проблемму, казалось что не определить режимы отделочного шлифования зеркально чистой поверхности.

Исходе из этого рассуждения мы взялись прежде всего, за основные опытно-эксперимантальные работаы.

2.1 Зависимость чистоты поверхности от окружной скорости обрабатываемой детали.

Теперь будем рассматривать зависимость чистоты шлифуемой поверхностиот изменения окружной скорости обрабатываемой детали по модели шлифования. При этом целесообразно взять модель шлифования, показанную на фиг. 9 в параграфе 1.2.5 (Зависимость чистоты шлифуемой поверхности от окружной скорости обрабатываемой детали), но фактически не только расстояние между зернами G0, G1, G2 значительно меньше, чем показано на фигуре, но и число оборотов шпинделя гораздо выше, чем показано на фигуре. Кроме того, для выполоения задали, поставленной в этом параграфе, допустимо взять другую модель шлифования, приближенную предыдущей, так как рассуждение по этой модели шлифования и о влиянии окружной скорости обрабатываемой детали не приводит ни к какому отрицательному результатату. Следовательно, ниже будем рассуждать теоретически но модели шлифования на **Фиг. 13**

Допустим, если вся поверхность круга представляет собои сплошные режущие кромки, то вся окужность, радиус которой O, A, соответствующая поверхностной форме круга, должна быть сплошными режущими кромками (см. фиг. 13, а). Иначе говоря если расстояние между режущими кромками равно нулю, то обрабатываемая деталь должна быть отшлифована всей этой периферией круга, т. е. когда обрабатываемая деталь совершит один оборот, то получится безукоризненная овальность без шероховатости, при этом центр овальности является O, а радиус-O, A.

Однако, фактически поверхностные зерна круга расположены произвольно и существует определенное расстояние. По модели шлифования, круг вращается с весьма большой скоростью. Предположем, что зерна на окружности имеют между собою определенное растояние G_1-G_2, и зерно G_1 (см,

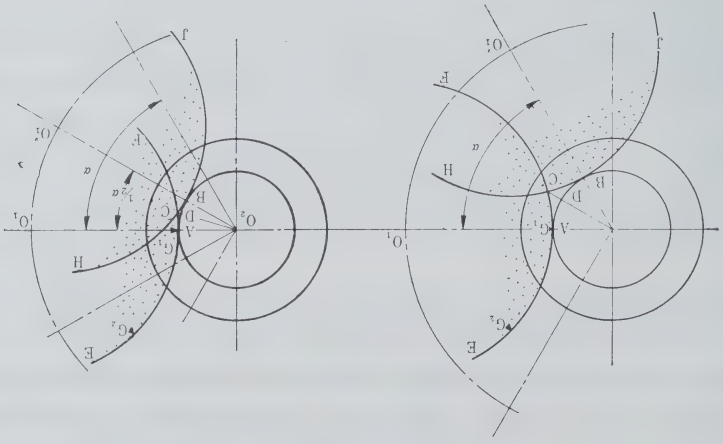

Фиг. 13 Зависимость чистоты шлифуемой поверхности от окружной скорости обрабатываемой детали (модель шлифования)

фиг. 13, а) осуществляет шлифование по периферии, приближенной к следу EAF в положении A, затем в положении B, в котором зерно G_2 прикаснется с обрабатываемой деталью, при этом следы последней и зерна приближенны к следу HBJ. Следовательно, нлощадь ABC, вписанная этими двумя следами - EAF, HBJ и окружностью, радиус которой O_2A, будет остаточным припуском зерна G_1 и G_2, т. е. растояние между D C/высота точки C / является шероховатосгью. При уменьшении числа оборотов шпинделя обрабатываемой детали в два раза, расстояние от D до C уменьшается в 4 раза (см. фиг. 13, в). Следовательно, чистота поверхности, безусловно улучшается. Из фигуры видно, что при увеличении окружной скорости в два раза, шероховатость шлифуемой поверхности в. 4 раза уменьшатся.

Правка круга производилась в след ющих режимах ;

Скорость правки круга / WA 46 LmV / 0,073 мм / об, врезная подача шарошек для правки 0,05 по диаметру 4 раза, 0,03 мм по диаметру 2 раза, 0,01 мм по диаметру 2 раза. Подавая смазочно-охлаждающую жидкость* Гангстаха на обрабатываемую деталь из материала S 45 C твердостью по Роквеллу 24 - 26, задавали постоянную врезную подачу на один оборот обрабатываемой детали 0,005 мм по диаметру и снимали припуск 0,5 по диаметру из заготовки диаметром 40 мм. На **Фиг. 14** показна зависимость чистоты шлифуемой поверхности обрабатываемой детали от изменения окружнй скорости обратываемой детали (7,5 м / мин, 15 м / мин, 30 м / минн).

Рассуждая по модели шлифования, видим гто увеличение окружной скорости обрабатываемой детали должно ухудшать чистоту шлифуемой поверхности, но при увеличении окружной скорости в два раза, все таки не должна быть ухудшена чистота шлифуемой поверхности в четыре раза.

* разведенная в 50 раз

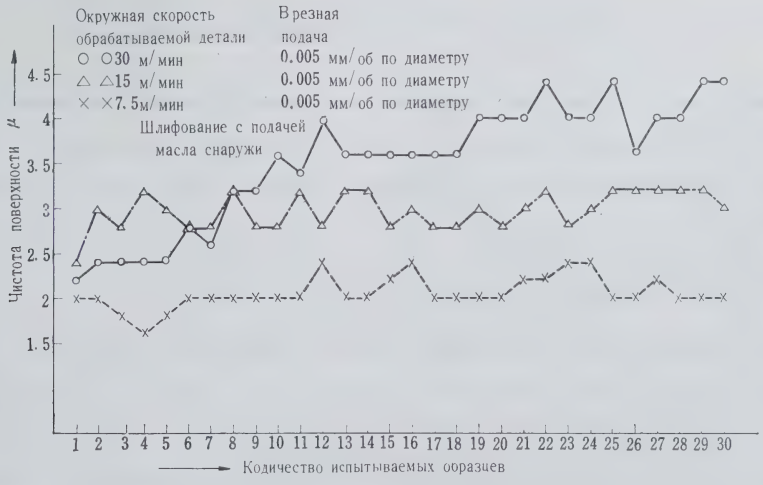

Фиг. 14 Зависимость чистоты шлифуемой поврхности от окружной. скорости обрабатываемой детали (S 450 твердостью по Роквеллу 24-26)

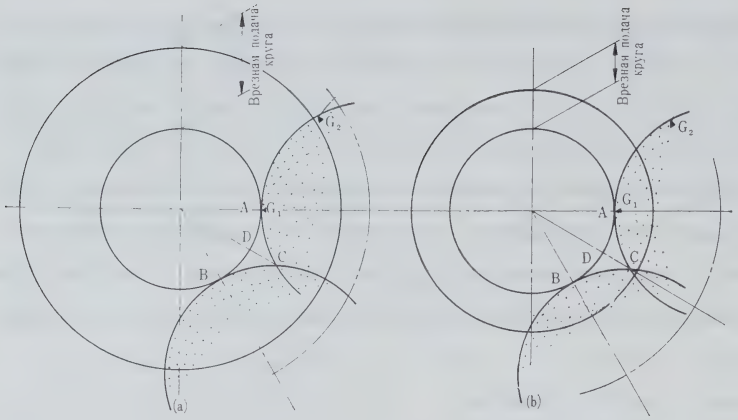

фиг. 15 Зависимосимсть чистоты шлиФуемой поверхности от врезной подачи круга(модель шлиФования)

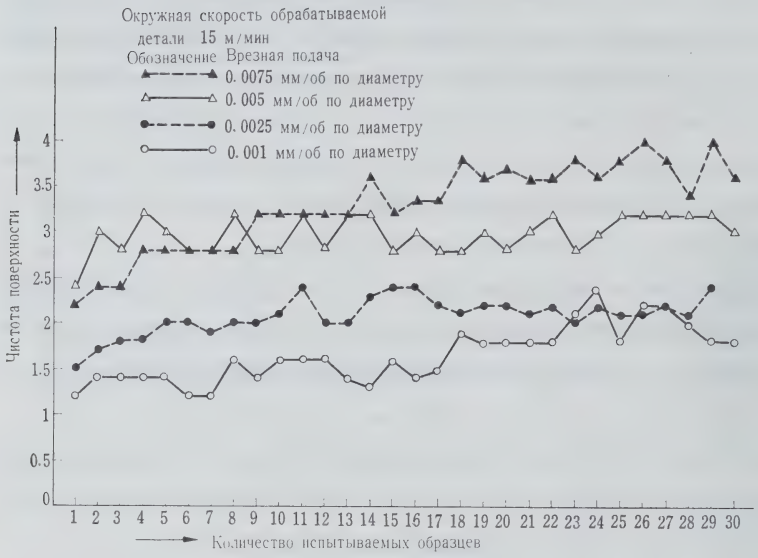

Фиг. 16 Зависимость чистоты шлифуемой поверхности от врезной подачи круга (S 45 C твердостью по Роквеллу 24-26)

2. 2 Зависимость чистоты шлифуемой поверхности от врезной подачи шлифовального круга

Ниже будем рассматривать зависимость чистоты шлифуемой поверхности от врезной подачи круга по модели шлифования на **Фиг. 15.** На **фиг.5, а** врезная подача круга в два раза больше, чем на. **фиг. 15,** в, а расстояние между D и C / шероховатость шлифуемой поверхности/ одинаково в том и другом случае. Другими словами, чистота шлифуемой поверхности не зависит от верзной подачи круга.

Круг, режимы правки круга, обрабатываемая деталь и припуск на шлифование те же как на фиг. 14(а). Задавая постоянную окружную скорость обрабатываемой детали 15 м/мин, производили шлифование с различными врезными на один оборот обрабатываемоой детали 0, 001, 0, 0025, 0, 005, 0, 0075 мм по диаметру. В результате этого шлифования получилась чистота шлифуемой поверхности обрабатываемой детали, а данные по измерению этой чсоты приведены на **фиг. 16.** Однако, по модели шлифования чистота шлифуемой поверхности должна быть одинаковой, поэтому она не состветствует

результатам этих этих экспериментов.

Взят материал для заготовки BsBM1, а другие условия - те же как указаны на фиг. 16, вследствии чего полученные данные экспериментов показаны на **фиг. 17.** Данные соответсвуют результатам по модели щифования, а они показывают, что чистота шлифуемой поверхности почти не изменяетя в зависимости от врезной подачи круга. Таким образом, данные по материалу BSBM1 соответствуют результатам экспериментов.

2.3 Соотношение самозатачивания круга и режимов шлифования

Сравнение фиг. 13 и 14, фиг. 15, 16 и 17 доказывает, что между материалом заготовки и шлифовальным кругом существует определенное соотношение. Это может быть, определенное изменение поверхностных зерен шлифовального круга зависит от материала заготовки.

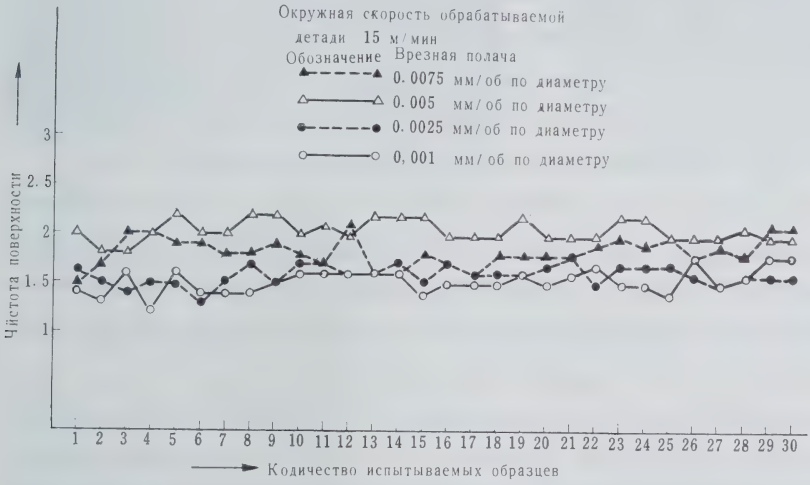

Фиг. 17 Зависимость чистоты шлифуемой поверхности от врезной подачи круга (BsBM1)

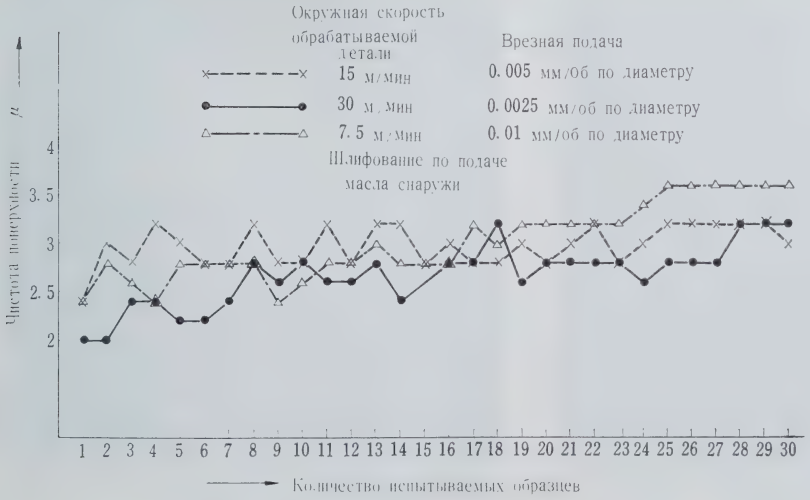

Фиг. 18 Чистота шлифуемых поверхностей при одинаковом количестве обработки в час (S45C твердостью по Роквеллу 24-26)

Всем известно, что строение шлифовального круга состоит из зерна абразива, связки и водушных промежутков – пор, и суть вопроса в том, что разиница зерен круга в прочности и твердости может быть оказывает влияние на чистоту шлифуемой поверхноти обрабатываемой детали. Самозатачивание круга, создаваемое этой разницей, будет расстоянием между поверхностыми зернами круга.

Еще раз производили опыт по материалу S 45 C при тех же условиях за исключением окружной скорости обрабатываемой детали и врезной подачи круга, но осуществлялось шлифование столько же, сколько в тот раз за определенную единицу времени, т. е. при окружной скорости обрабатываемой детали 7,5 м/мин, принята врезная подача 0,01 мм/об по диаметру, а при 15 м/мин-0,005 мм/об по диаметру и при 30 м/мин-0,0025 мм/об по диаметру. Результаты этого опыта показаны на **фиг.18.** Из фигуры видно, что при одинаковом количестве шлифования за определенную единицу времени, чистота шлифуемых поверхностей случайно получилась одинаковой. Почему случайно, потому, что на материале BSBM1 не появилось этого явления. Однако, из этих результатов следует, что расстояние между зернами круга, от которого зависит чистота шлифуемой поверхности,должно различаться в зависимости от режимов шлифования. Следовательно, зерна одно за другим разрываются или выпадают из-за силы сопротивления шлифованию, что приводит к непрерывному изменению зерен в процессе шлифования. В крайнем случае, из 10 зерен только одно участвует в операции шлифования.

В связи с этим, в целях узнать состояние режущих кромок и их разрыв в процессе шлифования зернами, снимали несколькими электронными микрофотографами поверхность зерен круга. На микрофотографах. №6 и 7 показываются примеры состояния режущих кромок.На микрофотографе показаны шлифовочные трещины большого разрыва в центральной части, в нижей части справа виден мельчайший разрыв кристалла.

Напристаример, зерно с зернистостью 60, которое состоит из тончайших кристаллов, в большистве случаев начинает разрываться при обычном шлифовании / не отделочном шлифовании зеркально

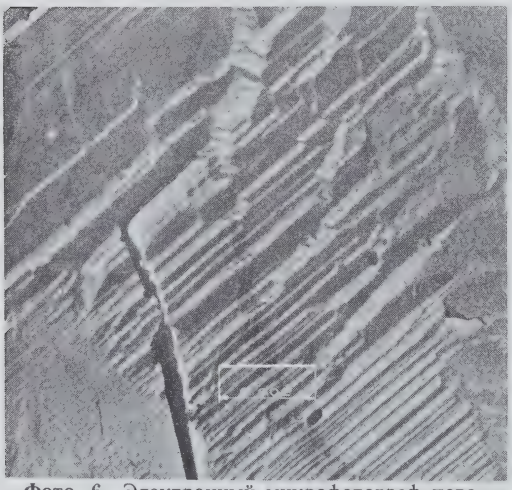

Фото. 6 Электронный микрофотограф поверхностных зерен круга

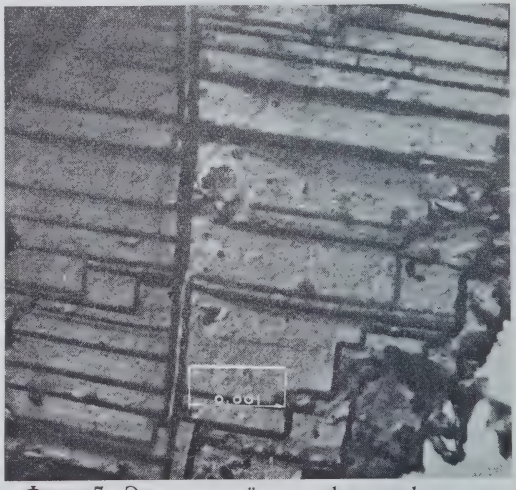

Фото. 7 Электронный микрофотограф поверхностных зерен круга

чистой поверхности на не мельчайшие кристаллы. Этот разрыв зависит от разницы врезной подачи или окружной скорости обрабатываемой детали, т. е. от усилия резания, воздействующего на зерно.

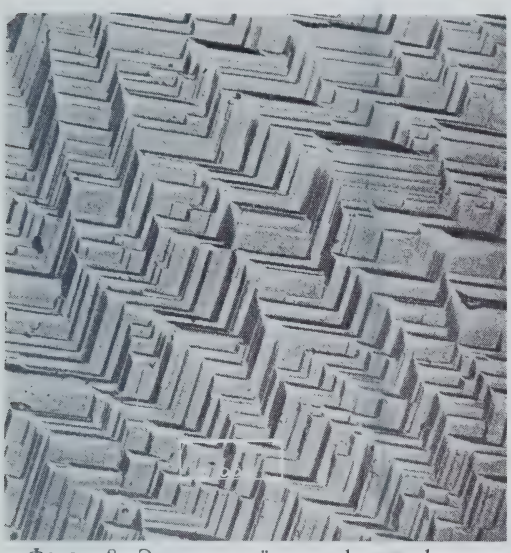

Фото. 8 Элеткронный микрофотограф поверхностных зерен мосле шлифования

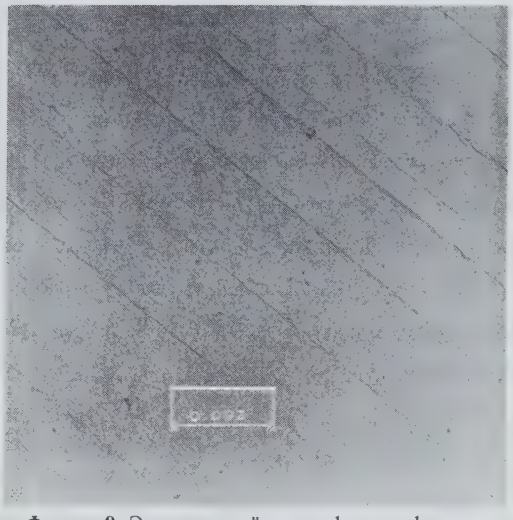

Фото. 9 Электронный микрофотограф шлифованной поверхности обрабатываемой детали одним зерном

3. Отделочное шлифование зеркальио чистой поверхности в третий период

Во вторй пепрнод было стремление к получению равномерных зерен подобно тому как у резца Геера и снятию незначительного припуска при шлифовании. Но, из электронных микрофотографов зерен видно, что зерна состгят из тончайших кристаллов и мы заметили, что последними возможно осуществить шлифование.

3.1 Шмифование микронными режущими кромками

Взамен круга нами разработан аллюминиевый диск, в котором вставлено одно зерно. Производили шлифование обрабатываемой детали в следующих условиях : окружная скорость зерна 30 м/сек, окружная скорость обрабатываемой детали 4 м/мин, режимы шлифования те же как при круглом шлифовании. После шлифовки сняли электронные микрофотографим зерен(см. **фотографию 8**) и шлифовочных рисок на поверхности обрабатываемой детали (**см. фотографию 9**)!

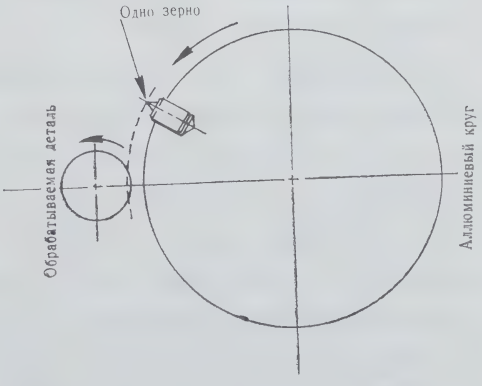

Фиг. 19 Схема шлифования одним зерном

Из этих результатов следует, что обнаруженные риски после шлифования на шлифовальной поверхности, образованы микрокристальными кро-

мками на задних зерен, от которых будто считалось не зависит качество шлифования.

3.2 Отделочное шлифование посредством самозатачивания круга

При черновой шлифовке сила резания, воздействующая на зерна велика, поэтому зернами должно быть осуществлено шлифование при режимах шлифования так, чтобы образовался разрыв (см. фотографию 7 посредине), а при чистовом шлифовании зеркально чистой поверхности уменьшается сила резания, воздействующая на зерна и осуществляется шлифование микрокристаллами, имеющими острые режущие кромки (см. фотографию 7 слева).

При последовательном шлифовании обрабатываемых деталей, не требуется правки круга, а увеличивая силу резания, воздействующую на зерна, существляют черновое шлифование. И так процеесы повторяются.

4. Выводы

Для чернового шлифования нужно увеличивать врезную подачу с учетом увеличения производительности труда. Для чистого шлифования зеркально чистой поверхности уменьшают врезную подачу круга и используют режущие кромки из тончайших кристаллов. Однако, вообще трудно определить соответствующее состояние разрыва зерен, так как оно зависит от врезной подачи круга, окружой скорости обрабатываемой детали, материала заготовки, прочности зерен и твердости круга.

На **фотографии 10** показан образец внутреннего шлифования с зеркально чистой поверхностью, чистоту которой можно определить в пределах 0,04 Hmax (0,04 S) - 0,02 Hmax.

При шлифовании по наружному диаметру на существующих станках фирма "Мицуи-Сэйки" достигла точность в пределах 0,04 Hmax, но до апреля 1962 года при внутреннем шлифовании с помощью круга WA 60 J фирма не смогла дать точность выше 0,05 - 0,1 мк Hmax. На фотографии 10 видно, что на внчтренней поверхности совсем отсутствует риска.

Как выше упомянуто, правильно выбирать режимы шлифования весьма трудно, и требуется много потрудиться над этим вопросом.

При шлифовании этого образца выабраны следующие режимы резания: скорость правки круга 0,07 мм/об, окружная скорость обрабатываемой детали 8 м/мин, врезная подача при черновом шлифовании 0,02 мм по диаметру на десять оборотов обрабатываемой детали. Уменьшая припуск на шлифование врезную подачу тоже уменьшали, затем задавали пять врезных подач круга по диаметру 0,001 мм в пределах

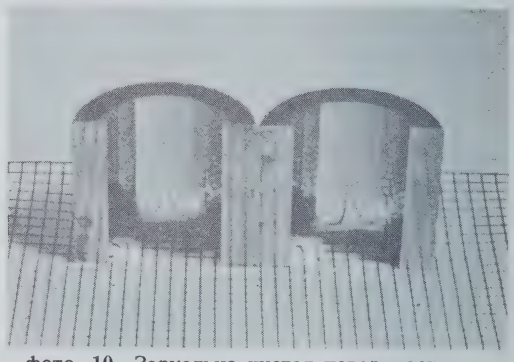

фото. 10 Зеркально-чистая поверхность внутреннего шлифования

фиг. 20 Чистота поверхности внутреннего шлифования

чистового шлифования зеркально чистой поверхности. В последней стадии отделана поверхность выхаживанием. При дальнейшем шлифовании второй или третьей заготовки не ребуется больше правки, а лишь повторять эти процессы. Таким образом, при черновом шлифовании используется визуальное самозатачивание круга, а при чистовом шлифовании зеркально чистой поверхности – микрорежущие кромки.

Этот метод мы называем отделочное шлифование зеркально чистой поврхности в третий период.

U.C.D. 621.315.592 : 620.186 : 621.923

Worked Layers of Optically Polished Surfaces of Semiconductor Crystals Viewed from the Ultra Micro-Scratching Hardness

Ichiro IDA, Yuzo ARAI, and *Makoto SUZUKI*

Reprinted from the
Review of the Electrical Communication Laboratory
Volume 11, Nos. 3–4, March–April 1963

THE ELECTRICAL COMMUNICATION LABORATORY
NIPPON TELEGRAPH AND TELEPHONE PUBLIC CORPORATION
535, 3-tyôme, Midori-tyô, Musasino-si, Tôkyô, Japan

U.D.C. 621.315.592 : 620.186 : 621.923

Worked Layers of Optically Polished Surfaces of Semiconductor Crystals Viewed from the Ultra Micro-Scratching Hardness*

Ichiro IDA,† *Yuzo ARAI*,‡ and *Makoto SUZUKI*‡

For the direct confirmation of worked layers on polished surfaces of semicondutor crystals, the ultra micro-scratching hardness tester has been constructed on a trial basis, with a diamond triangular pyramid used as the scratching tool. This tester can produce plastic scratching traces on brittle and hard materials at a load of 10–5,000 mg and a scratching speed of 4.5 mm/min, and the width of these traces being measured by an electron microscope.

By means of this tester, the scratching by a pyramidal face or by an edge of the diamond pyramid has been performed on the optically polished germanium and silicon.

As a result, hardness numbers have been obtained along the depths from the polished surfaces, and the characters of worked layers are discussed in view of the hardness distributions. The results obtained are as follows:

(1) The work softening exists in silicon to a depth of 700 Å, while the indication of softening is seen in germanium at a depth of less than 200 Å.

(2) The constant hardness numbers are found at a depth of 10,000–15,000 Å for both crystals, which is very close to that obtained from the etching rate curves.

(3) The softening phenomenon is caused by the temperature rises due to surface friction. According to a simplified model, the temperatures can attain up to softening points for both crystals.

Indroduction

Germanium and silicon are hard and brittle just as glass is at normal temperatures and pressures. In fact, lapped surfaces develop the typical conchoidal fractures.[1] Therefore, at an indenting load of 25 g which is generally used in a micro-hardness tester, brittle fractures occur on such crystal surfaces. Accordingly, not only the precise measurement of indentations is impossible, but also the indentations penetrate the polished layers, and these facts lead to the inapplicability of the so-called micro-hardness tester for the evaluation of polished layers.

If an extremely light load is applied to the microscopic region of the polished surface, and the hardness is obtained without brittle fracture, it will be possible to specify the character of worked layers due to the difference of materials or polishing methods, and also to suggest the mechanism of polishing.

Though the definition of hardness is not always clear, it relates at least to the strength in deformation. According to the conclusions by Tabor,[2] hardness has the close relation with the yield strength of a material. It can be very effective, if the worked layer is evalu-

* MS related to Sections 1 and 2 was received by the Society of the Precision Mechanics in Japan, 31, Oct. and to Sections 3 and 4 received on 19, Nov. 1962.

† Staff Engineer, Precision Technique Research Section.
‡ Precision Mechanics Research Section.

ated with this quantity—hardness. Brittle fractures can be avoided by combining ultra micro-load and microscopic area, for example, the indentation or the scratching by a very sharp diamond pyramid at a load of 10–5,000 mg on the polished surfaces. This process is a phenomenon of microscopic plasticity at high pressures. As pointed out by Brüche and others,[3] if a load of 1 kg is applied to an area of $10 \times 10\ mm^2$, $1\ kg/cm^2$, that is, the same as normal atmospheric pressure is produced. If the load and the length are reduced to one-thousandth, that is, if the load of 1 g is applied to an area of $10 \times 10\ \mu$, a pressure of $1,000\ mg/100\ \mu^2 = 1,000\ kg/cm^2 = 1,000$ atmospheric pressure will be produced. It means that the pressure becomes very high in spite of the very low load. In such a condition, brittle fractures due to the indentation or the scratching will not occur even in brittle meterials, because of the origination of the hydrostatic pressure. In view of plasticity, it is of course desirable that indentation hardness is used, but it is very difficult to find indentations because of their small sizes when produced by very light loads. The scratching hardness used here is considered to be a low-speed indentation hardness. In addition to this, it is shown that Mohs hardness, a kind of scratching hardness has a close quantative relation to Vickers hardness according to Tabor.[4]

Though considerable researches were found on the hardness of semiconductor crystals up to the present, loads used in them were comparatively heavy. Furthermore, hardness measurements were not always intended as the investigations of worked layers (in polishing). In this paper, the outline of this ultra micro-scratching hardness tester and the measuring methods of scratched traces are explained.

Then, the relations between the scratching load and the deformations on the optically polished germanium and silicon are covered, and the hardness distribution along the depth from the polished surface is indicated in considerations of dynamical and thermal effects.

1. Ultra Micro-Scratchings

It was necessary, for the object mentioned above, to construct the scratching hardness tester and to obtain the electron microphotographs of scratched traces. Therefore, these features will be described in more details.

1.1. The Ultra Micro-Scratching Hardness Tester

It is the most important matter in design that all guides should be constructed elastically without any rigid supports, because the very small loads and forces must be detected. According to the preliminary experiments, it was determined that a strain meter whose pick-ups used un-bonded type gages for measurements of loads and scratching forces, and bonded typed gages for measurements of scratching strokes, should be used. These quantities measured were all recorded by a pen-writing oscillograph.

The mechanism in the movement of the pick-ups is illustrated schematically in Fig. 1. By the fine movement of the modified body tube of a metallurgical microscope, the predetermined depth of indentation (load) is applied to the bar of the strain gage for measuring loads, a parts of which has a diamond scratching pyramid. When the scratching stroke is applied to the strain gage for measuring the horizontal forces, the relative displacement is produced on this strain gage, the sensitivity of which is four times higher than that of the gage for the loads. This pick-up for measuring the horizontal forces is guided by the two sets of the parallel springs, the object of which is also to support the pick-up. This part is connected with the stroke-producing part by the pin, while the intermediate leaf spring (fixing the strain gages) is moved with the reduction ratio of 1 : 20 by the linked lever shown on the left side of Fig. 1. The procedures mentioned above are applied in measuring three quantities of the load, force and stroke at the same time. This time, the load and the stroke are mainly measured. In this case, the specimen is set on the crosswise moving stage, in which the stroke of 1–1.5 mm

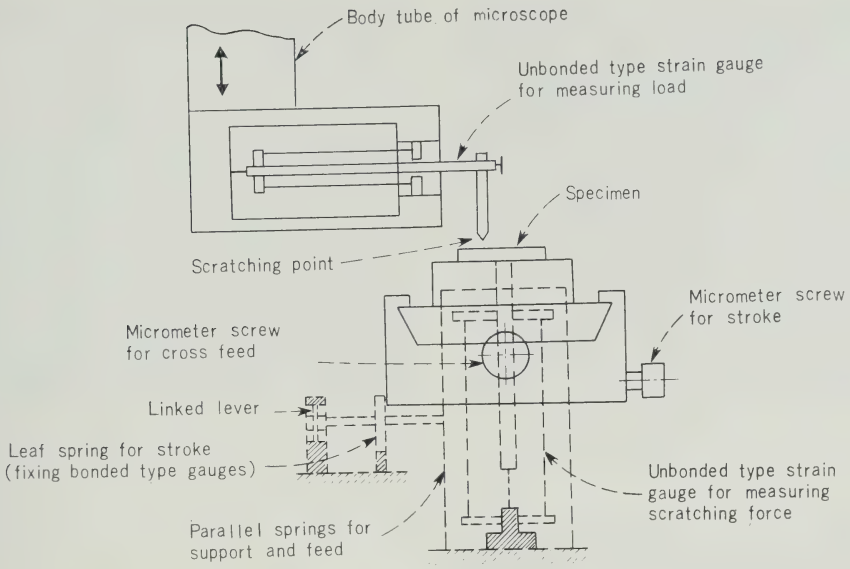

Fig. 1—Schematic mechanism of the movements in pick-ups.

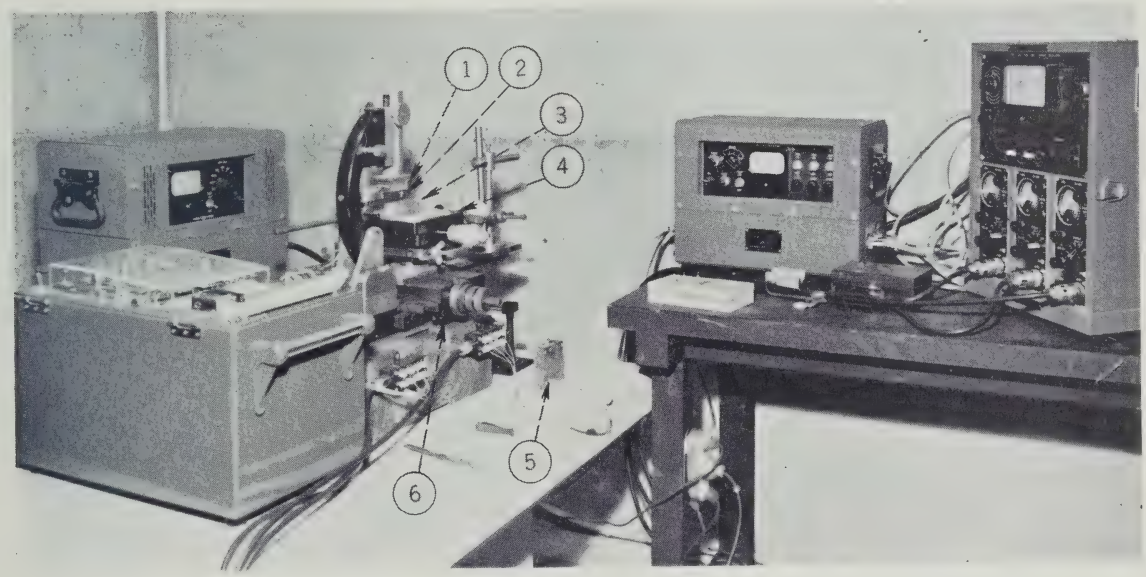

① Pick-up for measuring load. ② Diamond scratching point. ③ Specimen.
④ Crosswise moving stand. ⑤ Pick-up for measuring scratching force.
⑥ Modified carriage for cross feed when measuring three quantities of load, force and stroke.

Fig. 2—Outward appearance of the ultra micro-scratching hardness tester.

is applied by a micrometer screw, and the feed of 0.01 mm is applied by another micrometer screw. In the case of a simultaneous measurement for load, force and stroke, the cross feed was accomplished by the modified carriage of a lathe as shown in Fig. 2.

The next important matter is a scratching point. Since the ultra micro-load always correlates with the microscopic area, the point should be very sharp and have an ideal geometric shape. As well known, a square pyramid having the apex angle of 136° is used in a general Vickers micro-hardness tester. However, the machining of the single point on the top of a square pyramid is very difficult, because the accuracy of this geometric condition is very high, when measured in the microscopic region. In consideration of this difficulty, the triangular pyramid,[12] which is able to form a single point geometrically, is adopted here. The shape and dimensions are illustrated in Fig. 3 (a). In scratching experiments, there are two preceding directions of the diamond. One is the face and the other is the edge as shown in Fig. 3 (b). The former is expected to have a cutting effect, while the latter an effect of plastic deformation.[13]

The scratching apparatus was set on a wooden frame, which was furthermore put on a vibration-proof bed, together with the electrical measuring equipment, for prevention of external disturbances caused by vibrations and shocks.

1.2. Measurements of Scratching Points of the Diamond Pyramids

It is very important for us to find how sharp the radius of curvature of the diamond pyramid is. The dimension of the radius of curvavature should be measured by an electron microscope because the optical method is insufficient to obtain the quantative value in

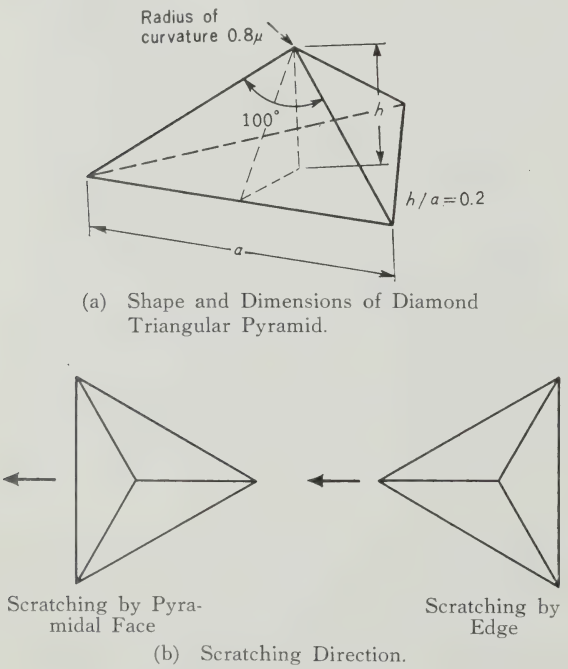

(a) Shape and Dimensions of Diamond Triangular Pyramid.

(b) Scratching Direction.

Fig. 3—Shape, dimensions and scratching dieections of a scratching point.

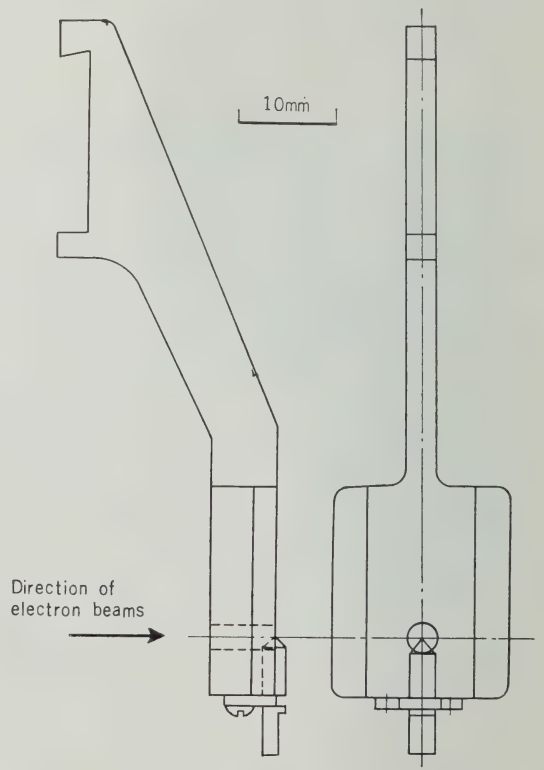

Fig. 4—Stylus holder.

* Concerning this matter, the authors are indebted to Mr. S. Hirota, a member of Circuit Component Research Section of this Laboratory.

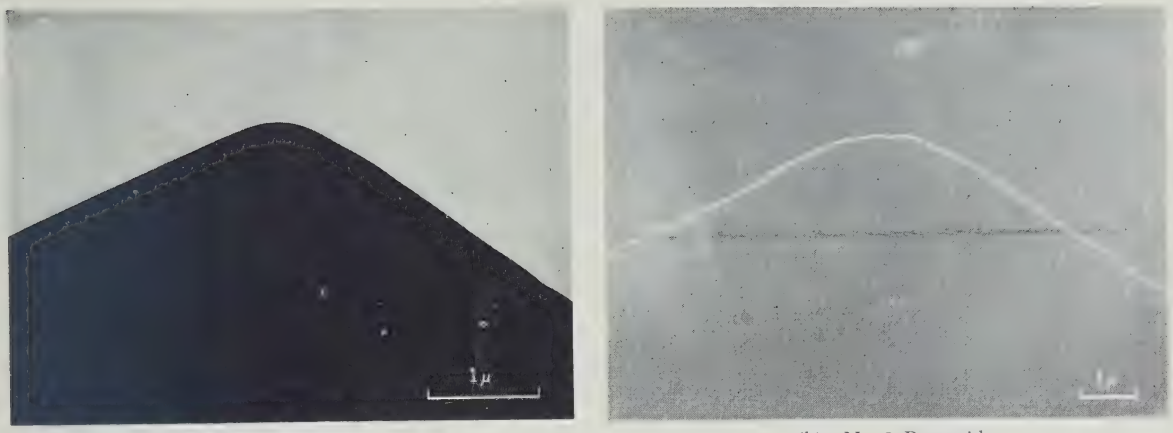

(a) No. 1 Pyramid. (b) No. 2 Pyramid.

Fig. 5—Projections of scratching points by electron microscope.

this case. However, the reduction of fidelity of a replica is serious because of the contraction of the relica. Therefore, measurements of the diamond pyramid are performed directly by the projection of electron beams. The procedure is realized by the special design of the stylus shape in order that the electron beams may irradiate The point of the stylus perpendicularly as shown in Fig. 4.

Examples of the projections are shown in Fig. 5. Fig. 5 (a) indicates that the electron beams irradiate the point perpendicularly as mentioned above, while Fig. 5 (b) demonstrates the dark field effect produced by the very small rotation of the stylus. Though two pyramids were prepared for the experiments, it was found that the No. 1 pyramid had a uniform radius and a flat pyramidal face, while the No. 2 pyramid had not only a rough surface, but also a "Dach" shape on the point. Of course, the No. 1 pyramid was used in the experiments, the radius of which was 0.8 μ†. The microscopic interference fringes showing the flatness of a pyramidal face is illustrated in Fig. 6.

Fig. 6—Microscopic interference fringes on pyramidal face of No. 1 pyramid.
(direct magnification ×60)

1.3. Measurements of Scratching Loads, Scratching Forces and Scratching Strokes

Inspections of items mentioned above were performed by the weights of a ultra microbalance and by a travelling microscope, and the linearity within 2% was confirmed among the readings and quantities measured as shown in the example of Fig. 7. The examples of the oscillograms for the scratching load and stroke are indicated in Fig. 8. These oscillograms were obtained from the following pro-

† The dimension was determined in comparison with the radii on negative plates of the electron microphotographs and the known radii of the optical template by the use of a tool maker's microscope.

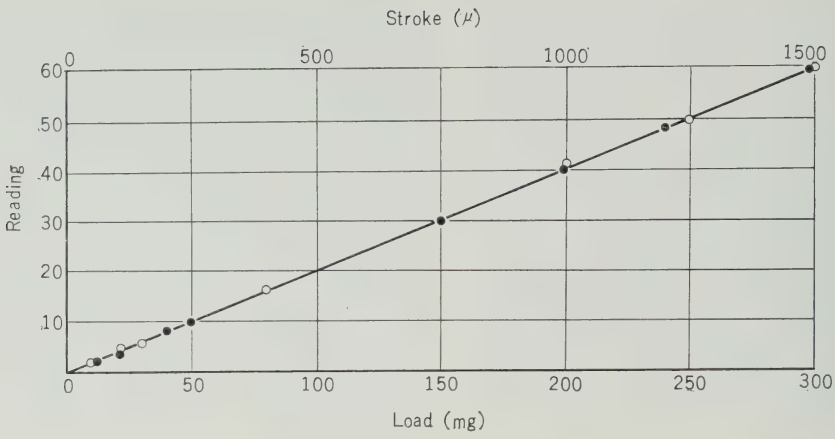

Fig. 7—Calibrations of scratching load and stroke.

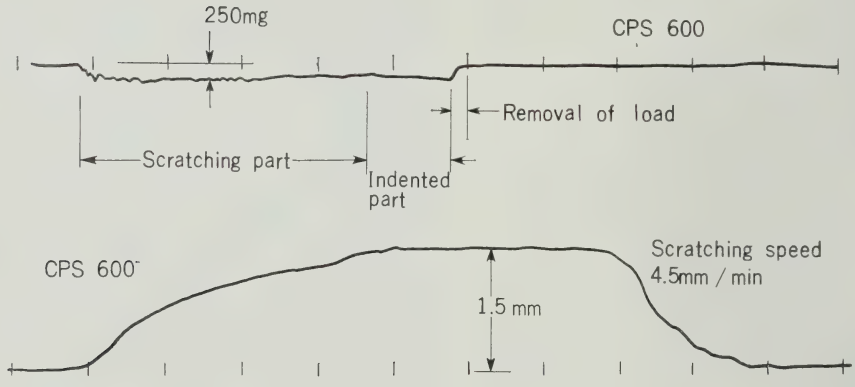

Fig. 8—Oscillograms of scratching load and stroke.

cedures. The modified body tube is lowerd slowly with a fine adjusting screw until the reading of the strain meter reaches the pre-calibrated value. Next, the specimen is shifted right or left for the distance of 1 mm, corresponding to the scratching directions by the stroke screw (or by the level), when the dial gage revolves one time. After giving the pre-determined stroke, the load is removed by lifting the body tube, and the cross feed of 0.01 or 0.015 mm is accomplished by the feed screw of a crosswise moving stage. Then the position of the specimen is moved back to normal, the confirmation of which is done by the dial gage. In this way, three or four scratched lines, including the standard line scratched at a load of 300 mg, are formed on the surface, Such a scratching method as this is useful to confirm the scratched traces when measured by an electron microscope.

Though the measurements of scratching forcess are not carried out regularly this time, the results obtained by the use of a sapphire stylus are shown in Fig. 9. It is seen that the coefficient of friction ($\mu=F_t/F_n$) is approximately 0.05.

It was found that the average scratching speed is about 4.5 mm/min, and this is easily reproduced by watching the revolutionary state of the pointer on the dial gage. Furthermore, the variation of the width was estimated to be less than 3% by the use of an electron microscope. Therefore, stroke were chiefiy accomplished by the micrometer screw and

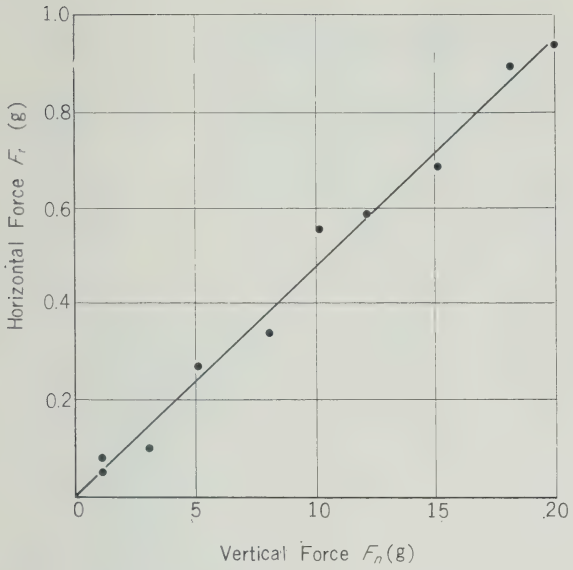

CPS 2,000, (111) surface of optically polished Ge, Sapphire, Stylus, radius of curvature 3 μ.

Fig. 9—An example of relation between vertical and horizontal force.

measured by the dial gage after the middle stage of the experiments. The accuracy of the cross feed has proved to be 5% in measurements of the phase contrast microphotographs under a magnification of $\times$1,200.

1.4. Measurements of Scratched Traces

When observed the parts of scratched traces thoroughly, the existences of traces can be detected up to a load of 200–300 mg. After marking with ink near the scratchings, and confirming the positions with a stereoscopic microscope under a magnification of $\times$120, three or four microphotographs are taken at a magnification of $\times$180, and about 15 photographs at a magnification of $\times$720 in series by the use of a phase contrast microscope.

There is no chance to misjudge the unscratched traces as the scratches ones, because the shapes of the traces and scratterings of chips are clearly found up to a load of 300 mg, when examined under a magnification of $\times$720, Though the existences of scratchings are scarcely shown at a load of the order of 10 mg, even if the phase plate (of negative high contrast) is used, the parallel lines can easily be detected as described previously.

Electron microphotographs are taken after scratchings, referring to the microphotographs taken by the phase contrast microscope, whose the method of obtaining replicas is the same as that described in the previous report.[14] Since the scratched traces correspond to the indentations at the start and the end of scratchings, the problems whether or not the indentation was carried out normally to the surface, and which is the start or the end of the scratchings can readily be determined.

1.5. Specimens

The specimens of an optically polished germanium having the (111) face were scratched in a definite direction. The scratching loads were chosen at six stages of; 5,000$\sim$3,000 mg, 3,000$\sim$1,000 mg, 1,000$\sim$500 mg, 500$\sim$100 mg, 100$\sim$50 mg and 50$\sim$10 mg.

2. Scratchings on Optically Polished Germanium

2.1. Scratchings by the Pyramidal Face

The whole or the part of the scratched traces are shown in Fig. 10, which were obtained from the phase contrast microscope. As seen from these photographs, serious conchoidal fractures are produced, and they cannot be the object for measurements at loads of over 5,000 mg. Conchoidal fractures are produced at intervals of 5–10 μ at a load of 5,000 mg, the chips of which are block shaped, having a size of 0.5–3 μ. Therefore, it is clear that the fractures in tension occur in this range of the load. The variation of scratching loads amounts to 10% in this case. Though the brittle fracture are originated partially at a load of 1,000 mg, the plasticity of germanium is seen at this load, because the trace previously scratched is erased by the one scratched later on. This appearance is illustrated in Fig. 11 in details. When observing the phase contrast microphotographs after making replicas, the chips mentioned above hardly appear, which tells us that the chips were small

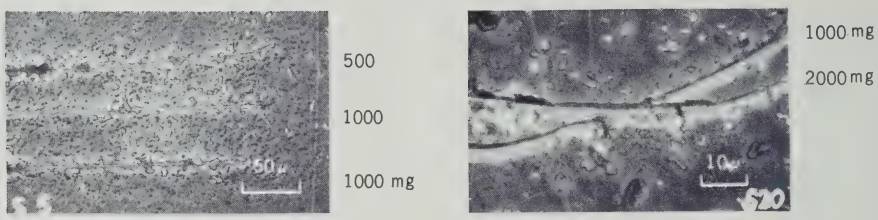

(a) At High Load, before making Replicas.

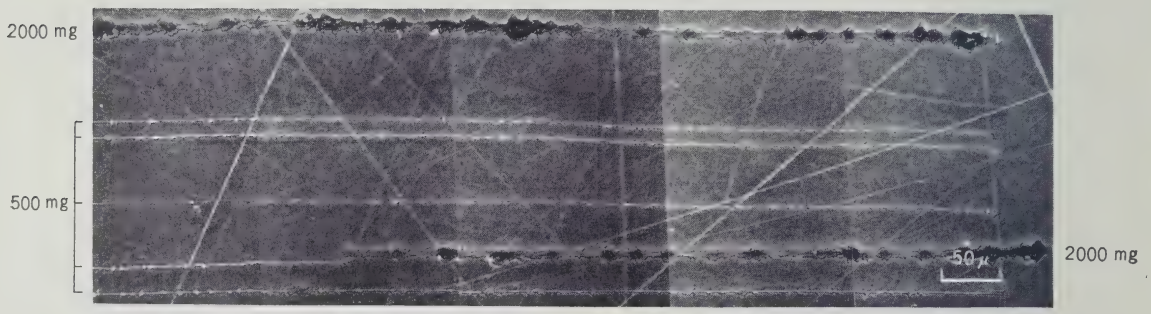

(b) At High-middle Load, after making Replicas.

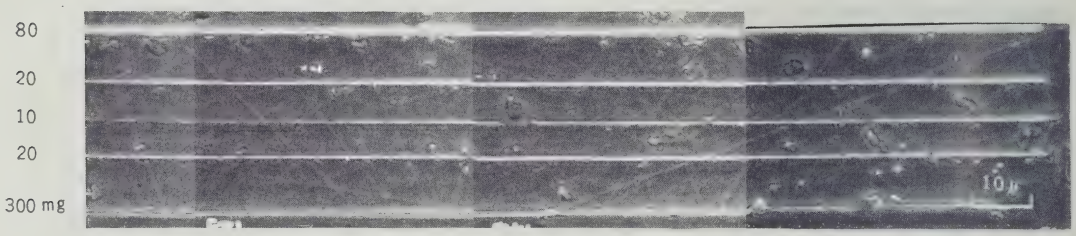

(c) At Low Load, before making Replicas.

Fig. 10—Phase constrast microphotographs of scratchings by pyramidal face on optically polished germanium.

pieces caused by scratchings.

At a load of 500 mg, the sizes of chips become about 0.5 μ, and the pitch of the conchoidal fractures extends to 20 μ, which shows the more difficulty of origination of brittle fracture. In Fig. 10 (b), scratched traces at loads of 500 and 2,000 mg are shown.

On the other hand, at a load of 300 mg, the scratchings behave plastically when observed by the phase contrast microscope. As shown in Fig. 10 (c), narrow and long chips are produced in addition to the continuous scratchings, which suggest the existences of the chips formed by "shear" under the action of a scratching point. From this point of view, the domain at this load seems to differ essentially from that at over 1,000 mg. In the case of the scratching by a pyramidal face, the cutting effect should be large, and this effect is confirmed with the result that small chips exist near the scratched traces even at a load of 10–20 mg. Moreover, these chips curl, which means the process of the cutting action. In other words, the smaller the loads become, the more frequently the flow-type chips are originated.

Next, the aspects of originations of scratched traces were examined by an electron microscope. Though the conchoidal fractures originate at a load of 5,000 mg as shown in Fig. 12 (a), sheared marks are found at the sides of cut traces, the pitch of which are about

Fig. 11—Electron microphotograph showing cross of both scratched traces by pyramidal on optically polished germanium.

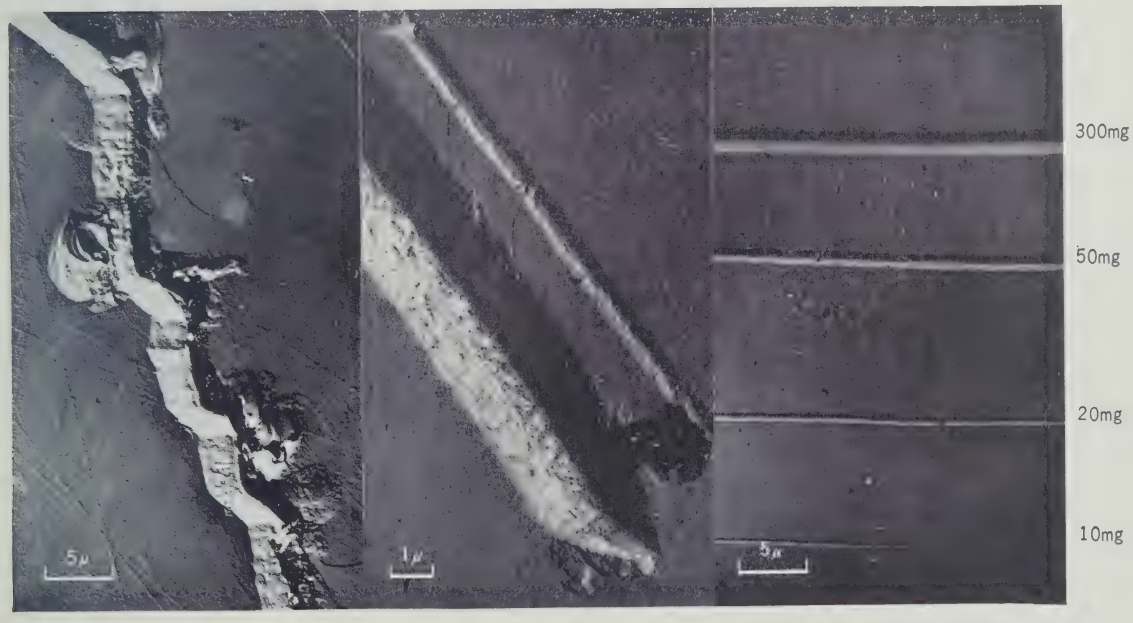

(a) At High Load, 500 mg (b) At Middle and Low Loads, 800 and 50 mg (c) At Low Load

Fig. 12—Electron microphotographs of scratched traces produced by pyramidal face on optically polished germanium.

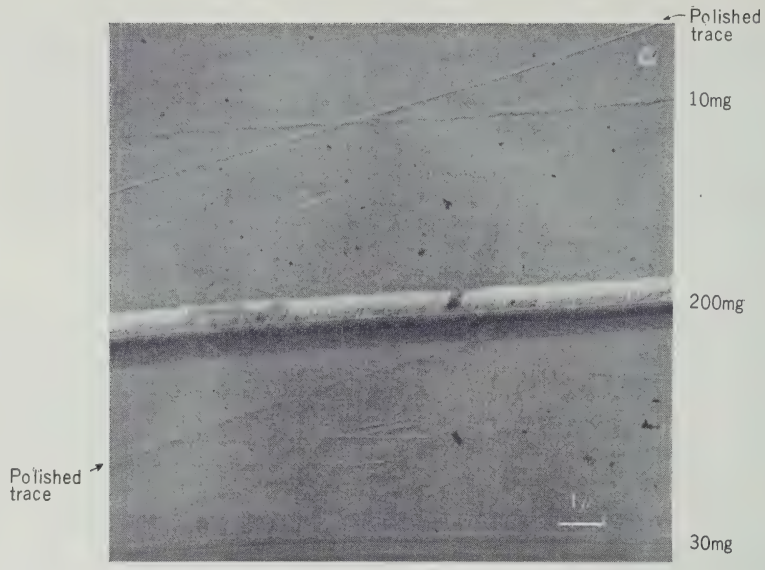

Fig. 13—Electron microphotographs showing cross of scratched trace produced pyramidal face and polished trace on optically polished germanium.

1.5 μ. At a load of 1,000–800 mg, the 'pile-ups' of materials at the walls and the adhesions at the edges are notable. As seen from Fig. 12 (b), the scratching is proved to be formed normal to the surface, because the symmetric pattern of a scratching end is caught at the start of the scratching. Also, the secondary hair cracks are seen in this photograph, the pitch of which is evaluated to be about 1 μ. At loads of 100 mg or less, brittle fracture is hardly found, and also the the origination of hair cracks are not seen as shown in Figs. 12 (b) and 12 (c), which mean the the perfect plasticity of germanium. In comparison with the photograph shown in Fig. 15 (c), it is clear that the ‚pile up' is rather small, because the edge is clearly defined. When examining the scratched traces caused by a load of 10–20 mg under the direct magnification of $\times$10,000, the widths of the 'pile ups' are less than one fifty of those of the scratched traces.

The crossed trace between the trace produced by polishing and the one produced by scratching at a load of 10 mg is shown in Fig. 13. Since the trace produced by polishing is entirely erased by the scratching, it may be conducted that plastic deformation occurs. Moreover, in comparison with the width of each scratch, the load applied on one abrasive in the course of polishing seems to be less than 3 mg, probably in the order of several tenths of a milligram.

Summarizing the results obtained from the phase contrast and electron microscopies, the relation between the range of the loads and the domain of deformations is indicated as follows:

Elastic region ·····less than 10 mg
Plastic region ·····10 to 100 mg
Plastic and secondary flaw region
·····100 to 300 mg
Plastic and cutting region
·····300 to 1,000 mg
Cutting and fracture region
·····1,000 to 5,000 mg
Fracture region ·····over 5,000 mg

2.2. Scratchings by the Edge

In the case of a scratching by the edge, there exists no cutting edge in the diamond pyramid as easily be understood in consideration of the geometrical shape, because the preceding front of the pyramid is constructed with the edge formed by two pyramidal faces.

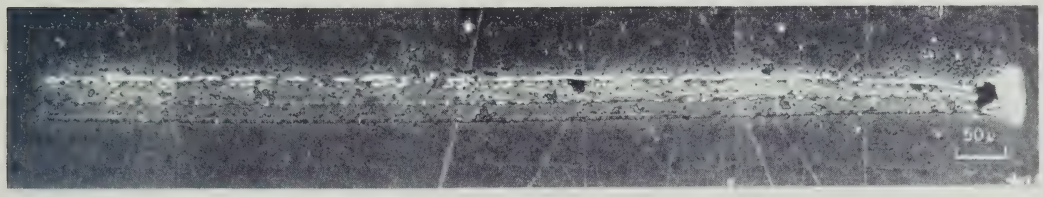

(a) At High Load, before making Replicas.

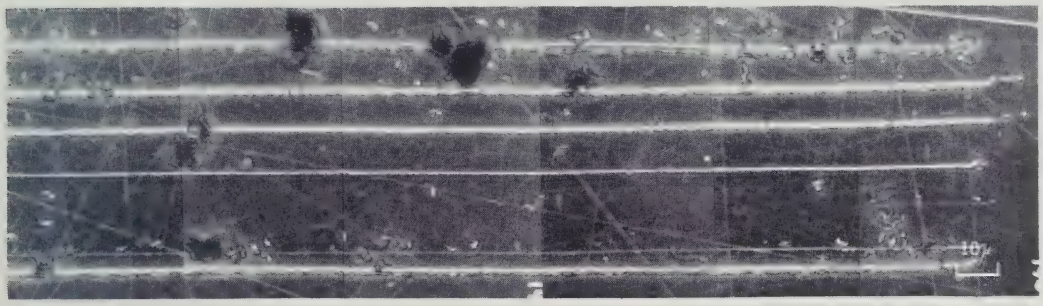

(b) At Middle Load, before making Replicas.

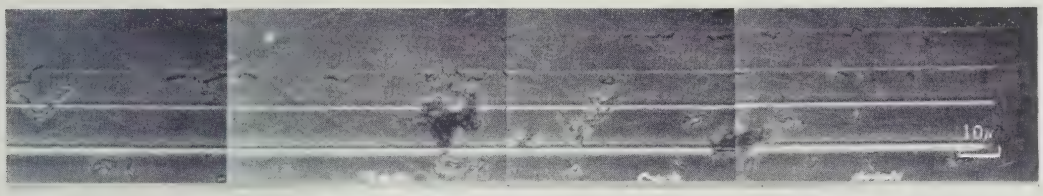

(c) At Low Load, before making Replicas.

Fig. 14—Phase contrast microphotographs of scratchings by edge on optically polished germanium.

That is, only plastic deformation should be produced on the surface ideally. However, the cutting components appear actually due to the very small deviation of scratching directions, and also the fracture in tension is produced at higher loads. Therefore, there exist more or less scratches even in this case.

These two pyramidal faces compress the material downwards and form 'pile-ups' at both sides of a scratching as the result of plastic deformation. Therefore, it can be said that the cutting effect should be even smaller. This phenomenon is clearly shown in Fig. 14. It is found that the chips continue especially at one side of a scratching in spite of the high load, and that conchoidal fractures of large sizes and the closely lined pitch are not seen as in the case of scratchings by the pyramidal face. However, small block-shaped chips are also found locally at the other side of a scratching. The non-existence of a cutting edge is demonstrated by the fact that the scratching cannot proceed at a load of 5,000 mg, unless the effective load decreases.

As shown in Fig. 14 (b) which illustrates the scratches at the range of middle loads (100–700 mg), the tendency mentioned above is furthermore produced. The chip produced by the cutting component curl more strongly than those produced by the pyramidal face. These results manifest the stronger effect of plasticity. Actually the surface deforms plastically due to compression under the two pyramidal faces when scratched.

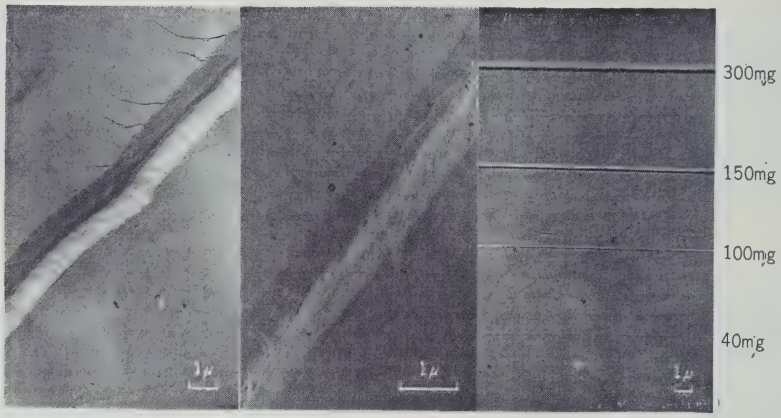

(a) At High Loud, 1500 mg (b) At Middle Load, 700 mg (c) At Low Load

Fig. 15—Electron microphotographs of scratched traces produced by edge on optically polished germanium.

It can be said on the whole, that scratchings at a load of 100 mg produced by a pyramidal face correspond to those at a load of 300 mg produced by an edge. In the case of the range of low loads, the tendency mentioned above is strongly acceralated, where the long curled chip has a length of 10 μ. It is concluded that the effect of plasticity is very large as expected in scratchings produced by an edge, accompanying the results of very few fractures even at a load of 1,000 mg.

When examined under an electron microscope, the aspects of scratched traces are clearly confirmed to be plastic without breakage even at the same load as in the case of scratchings by a pyramidal face. For example, as seen from the scratchings at a load of 1,500 mg in Fig. 15 (a), this trace is quite smooth, of which the aspect corresponds to that of the trace scratched by a pyramidal face at a load of 800 mg. It is also noted that the width of a scratching is small because the material removed is small due to a smaller cutting component. This tendency is the same as in the scratchings at a load of 2,000 mg, except for the existance of hair cracks, the lengths of which are about 2 μ. At a load of 3,000 mg, the concoidal fractures are displayed locally and the hair cracks increase their lengths to about 5 μ. This increase is nearly proportional to the scratching load. From these results, it can be said that the limit without hair cracks is 500 mg, and the observations by an electron microscope tell us this is true. Moreover, a short hair crack having a length of about 0.5 μ is seen at a load of 700 mg as shown in Fig. 15 (b), which also satisfies the relation mentioned above (refer to Fig. 16).

In the range of middle loads, no hair cracks exist any more, which mean the plastic deformation, accompanying the aspects that the

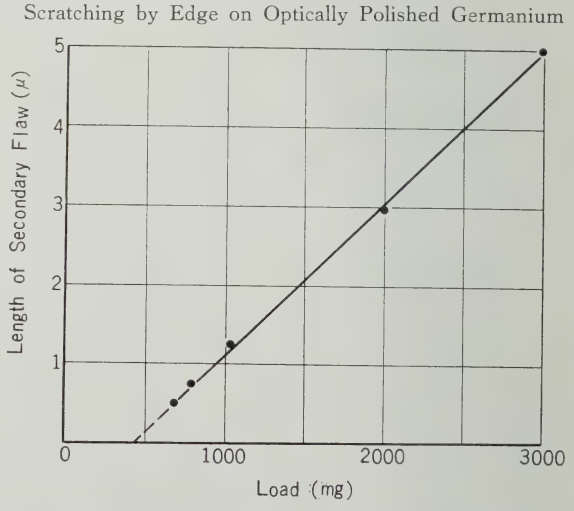

Fig. 16—Relation between length of secondary flaw and load.

boundary between the edge and the polished surface is obscure, and that the 'pile up' exist at the sides of the scratchings. The sizes of the 'pile ups' become one fifth of the width (at a load of 500 mg) to one eighth (at a load of 800 mg), respectively. The increase of the 'pile up' is explained as the decrease of the effect of cutting, because the lower load has less effect of cutting.

On the other hand, at low loads, the decrease of the width in the scratching is notable as seen from the comparison between Fig. 12 (c) and Fig. 15 (c), that is, the effect of plastic deformation is stronger in the latter case. Moreover, it is especially noted that the 'pile up' is larger, which has no 'shear mark' as shown in Fig. 17. At a load of 100 mg, the width of the 'pile up' reaches one-fourth of the that of the scratch.

As treated in the case of the the scratchings by a pyramidal face, the relation between the range of the the loads and the domain of the deformations is summarized as follows:

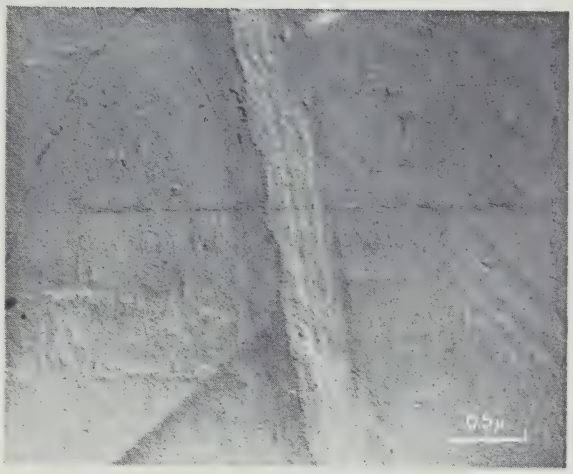

Fig. 17—Electron microphotograph showing effect of plastic deformation produced by scratching at 300 mg with edge on optically polished germanium.

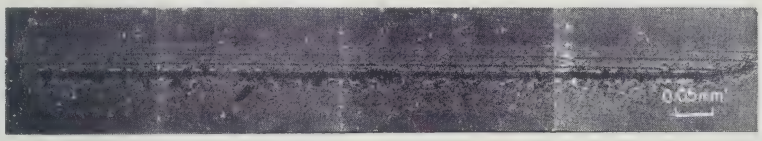

(a) At Medium High Loads, before making Replica.
Scratches at Loads of 800, 800, 1,500, and 3,000 mg from Above.

(b) At High Loads, before making Replica.
Scratches at Loads of 2,000, 1,000, and 4,000 mg from Above.

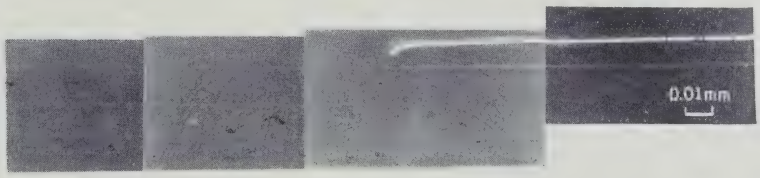

(c) At Low Loads, after making Replica.
Scratches at Loads of 300, 10, 20, 10, and 10 mg from Above.

Fig. 18—Phase contrast microphotographs of scratched traces by pyramidal face optically polished silicon.

Elastic region·····less than 40 mg
Plastic region·····40 to 700 mg
Plastic-secondary flawed region
·····700 to 1,000 mg
Plastic-cutting region····1,000 to 3,000 mg
Plastic-fractured region··3,000 to 5,000 mg
Fractured region ·····over 5,000 mg.

3. Scratchings on Optically Polished Silicon

It is said that the hardness of silicon is higher than that of germanium according ot the conventional data, namely, it is 950 Kg/mm^2 for silicon and 750 Kg/mm^2 for germanium.[8] However, on the optically polished surfaces, softening is expected to occur because of the frictional heat that occurs when optically polishing to a mirror surface, as already covered in the previous paper.[14]

3.1. Scratchings by the Pyramidal Face

At a higher load, the brittle fractures, similar to those in germanium, are shown in Figs. 18 (a) and 18 (b), where the scrattering of chips and the origination of the conchoidal fractures especially at a load of over 3,000 mg are seen. On the otherhand, considerable smooth scratchings are found at a medium load of 800 mg, illustrating the noticeable plastic effect as shown in Fig. 19 which was taken after replica making. As shown in Fig. 18 (c), brittle fractures are rarely found at lower loads. Though the tendency mentioned above is not generally different from that in germanium, the scratchings seem to be more smooth than those in germanium at medium and low loads. This is confirmed by the next electron microphotographs.

As seen from the examples shown in Fig. 20, it is noted that the adhesion of materials and the 'pile-ups' are more active, and the 'shear marks' appear more clearly in silicon

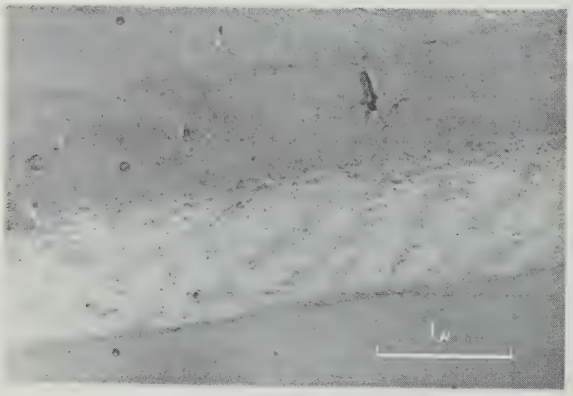

Fig. 19—Effect of plastic deformation in scratched trace produced by pyramidal face at a load of 800 mg on silicon.

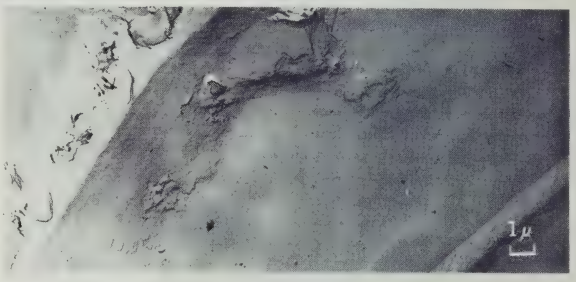

(a) Traces scratched at Loads of 3,000 mg (Left) and 1,000 mg (Right).

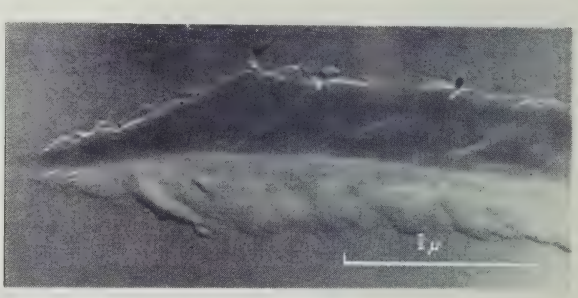

(b) Traces scratched at a Load of 230 mg.

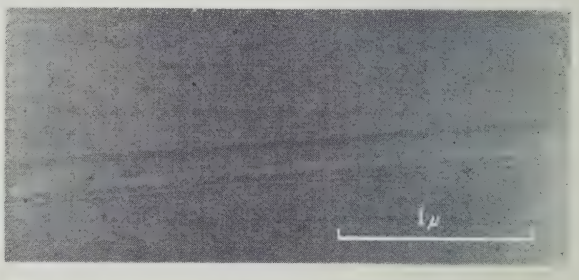

(c) Traces Scratched at a Load of 10 mg.

Fig. 20—Electron microphotographs of scratched traces produced by pyramidal face on optically polished silicon.

in spite of the pyramidal face having the larger cutting component.

At a load of 3,000 mg, there are stock removals of the material by the cutting edge, because the scratched traces have no 'pile-ups' at the edges, the 'shear marks' of which have a nearly constant pitch and have hair cracks correlating closely with the pitch. However, the aspect of the scratchings at a load of 1,000 mg is very much the same as those of the scratchings at a load of 800 mg or so, which shows the decrease of fractures in comparison with the scratchings in germanium. The remarkable features of scratchings at a medium load are that the adhesion of materials and the 'pile-ups' are very clear as shown in Fig 20 (b), indicating the large effect of plastic deformation. The width of 'pile-ups' are larger than those of germanium, having approximately one-ninth of that of the scratched trace. This observation suggests that the secondary effect may be the thermal softening.

At a lower load, the material is considered to be almost plastic, because the widths of 'pile-ups' reach one-fourth to one-eigth of those of scratches at a load of 10–85 mg and the 'shear marks' are not as clear as those in germanium. Moreover, the length of secondary flaws is 0.2 μ, and is no more than one quarter to one half of those found in germanium at a load of less than 800 mg.

As treated in the previous cases using germanium, the results mentioned above are summarized as follows:

Elastic region	less than 15 mg
Plastic region	15 to 400 mg
Plastic and secondary flaw region	400 to 1,000 mg
Plastic and cutting region	1,000 to 3,000 mg
Cutting and fracture region	3,000 to 5,000 mg
Fracture region	more than 5,000 mg

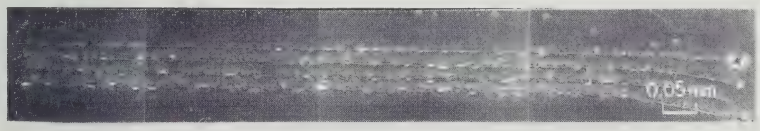

(a) At High Loads, after making Replica.
Scratches at Loads of 2,000, 3,000, 4,000, and 5,000 mg from Above.

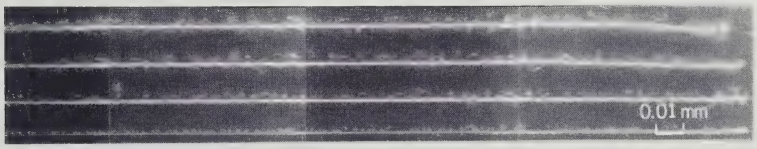

(b) At Medium Loads, before making Replica.
Scratches at Loads of 1,000, 800, 600, and 400 mg from Above.

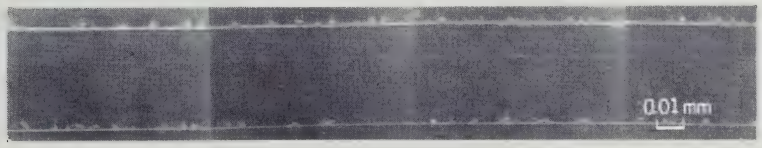

(c) At Low Loads, before making Replica.
Scratches at Loads of 250, 150, 85, and 250 mg from Above.

Fig. 21—Phase contrast microphotographs of scratched traces by edge on optically polished silicon.

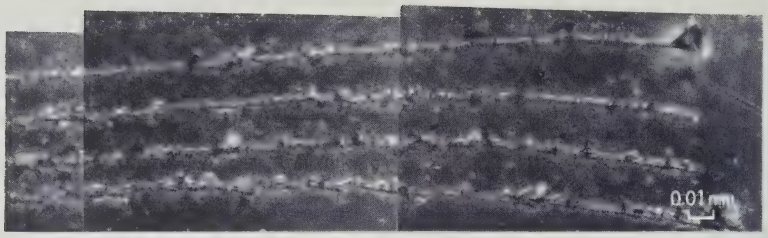

At High Loads, before making Replica. Scratches at Load of 2,000, 3,000, 4,000, and 5,000 mg from Above.

Fig. 22—Phase contrast microphotograph of scratched traces by edge on optically polished silicon.

3.2. Scratchings by the Edge

Though the conchoidal fractures occur at an interval of nearly 20 μ, comparatively smooth scratchings are originated between the fractures and indicate a similar effect of plasticity and cutting as that in germanium (Fig. 21). Particularly, at a load of 3,000–4,000 mg, the origination of chips towards one side of a scratching is characteristic as shown in Fig. 22. Most of the chips are long curled, when produced by a medium load, as shown in Fig. 21 (b), where the conchoidal fractures are very small. The degree of curling is stronger than that in germanium. It can be seen in comparison with the scratching at a load of 1,0000 mg shown in Fig. 14 (b). At a load of 85–150 mg. there are hardly any chips as illustrated in Fig. 21 (c). These facts suggest that scratchings are originated only by plastic deformation at the loads mentioned above. At a slight high load of 250 mg, the 'pile-ups' towards one side of the scratching are found similar to those found in germanium.

When observing the electron microphotographs of scratched traces, the higher effect of plasticity-cutting, that is, the existence of risings on the wall of a scratching and the non-existence of secondary flaws are found even at a high load as shown in Fig. 23 (a). At a medium load, it is noted that the secondary flaws do not exist and the 'pile-ups' are formed at the walls and the edge of the trace. The smaller the load is, the more strongly this tendency is demonstrated, especially, the continuous formation of chips exists at the side of a scratching in a direction

(a) Trace, scratched at a Load of 2,000 mg.

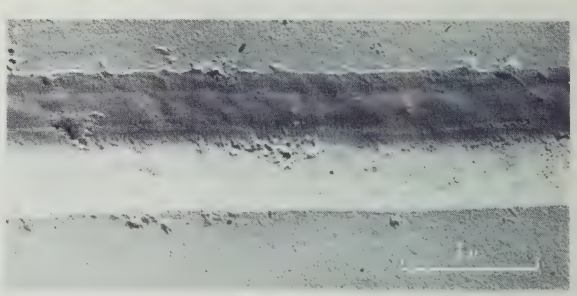

(b) Trace scratched at a Load of 800 mg.

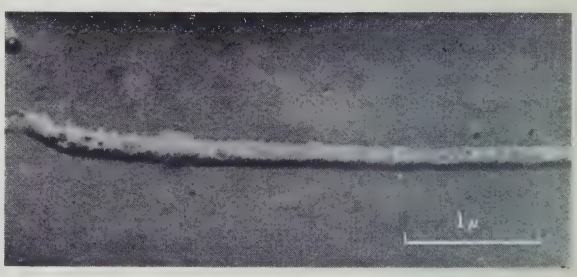

(c) Trace scratched at a Load of 20 mg.

Fig. 23—Electron microphotographs of scratched traces produced by edge on optically polished silicon.

Table 1

RELATIONS BETWEEN SCRATCHING LOADS AND RANGES OF DEFORMATIONS ON OPTICALLY POLISHED SURFACES

(mg)

Scratching by	Material	Elastic	Plastic	Plastic-Cutting	Cutting-Fracture	Fracture
Pyramidal Face	Ge	<10	10- 100	100–1,000	1,000–5,000	> 5,000
	Si	<15	15- 400	400-3,000	3,000–5,000	> 5,000
Edge	Ge	<40	40- 700	700–3,000	3,000–5,000	> 5,000
	Si	<18	18–1,000	1,000–3,000	3,000–5,000	> 5,000
Glass*		<10	10- 500	500–1,000	——	>10,000

* E. Brüche: Glastechn. Ber., Jg. **27** (1954) s. 239.

normal to its width. Because of this phenomenon, the fine structure of a scratching seems to be obscure, generally having a noticeable rising at the wall, when the pitch is about 0.06 μ. Moreover, the polished trace is entirely erased by the scratched one at a load of 18 mg as shown in Fig. 24. Therefore, it can be said that the non-existence of chips found on the phase contrast microphotographs means the scratchings was caused by plastic deformation. In other words, the scratching at a low load gives the risings showing the result of plastic deformation which is the displacement of materialat the wall, while the conversion of this to the 'shear mark' takes place as the load is higher.

Fig. 24—Crossing of scratched trace produced by edge at a load of 18 mg and polished trace.

The relation between the range of loads and the regions of deformations is summarized as follows:

Elastic region ····· less than 18 mg
Plastic region ····· 18 to 1,000 mg
Plastic-secondary flaw-cutting region ····· 1,000 to 3,000 mg
Cutting-fracture region ·· 3,000 to 5,000 mg
Fracture region ····· more than 5,000 mg

The total result obtained from the microscratchings on optically polished germanium and silicon is given in Table 1. From this, it is concluded as follows:

(1) Silicon is more plastic than germanium at the skin of the polished surface.

(2) The scratchings caused by the edge creates much stronger plasticity than scratchings caused by the pyramidal face.

(3) Loads of over 5,000 mg produces brittle fractures on both types of crystals.

4. Worked or Deformed Layers in View of Scratching Hardness

From the measurements of scratched widths,

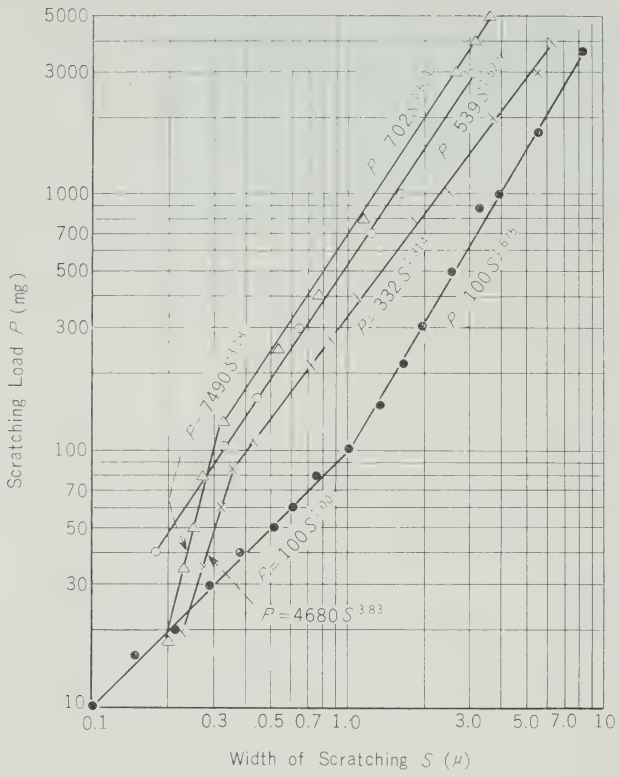

● Scratching by pyramidal face on Ge.
○ Scratching by edge on Ge.
× Scratching by pyramidal face on Si.
△ Scratching by edge on Si.

Fig. 25—Relation between scratching load and width of scratching.

the hardness number is calculated, using the following equation:

$$H = \frac{4}{\pi}\left(\frac{P}{S^2}\right),$$

where P is the load and S scratched width. The above equation is to calculate the Meyer hardness number. This calculation is of course approximate, and it should be amended in consideration of the penetrating depth and the influencely of the radius of curvature of the diamond pyramid. However, when the relative values are treated, the above equation will sufficiently be accurate. In addition, the depth of a scratched trace, h, is obtained from the next geometrical relation.

$$h = 0.2S.$$

4.1. Ultra Micro-Scratching Hardness

The relation between the scratched width S and the scratching load P is indicated in Fig. 25. In comparison with the indices n, the following items will be clarified. The two kinds of the load ranges are found in both types of crystals, and the n of silicon is very large. When comparing the extended curve at a higher load with that at a lower load, the wider width of scratchings is found on the curve at a low load. which leads to the softening of silicon in the first region.

On the other hand, the value of n does not indicate the constant tendency in the second range. As described previously, the difference between scratchings by the pyramidal face and the edge is produced by the effect of cutting or the effect of plastic deformation. Even though the chips have long curled shapes and the 'pile-ups' become large in the case of plastic deformation, these facts do not mean the absence of the cutting component, so long as the material is removed as thechips. Namely, the process is a mixture of both the the effects, but the degree of a mixture is different

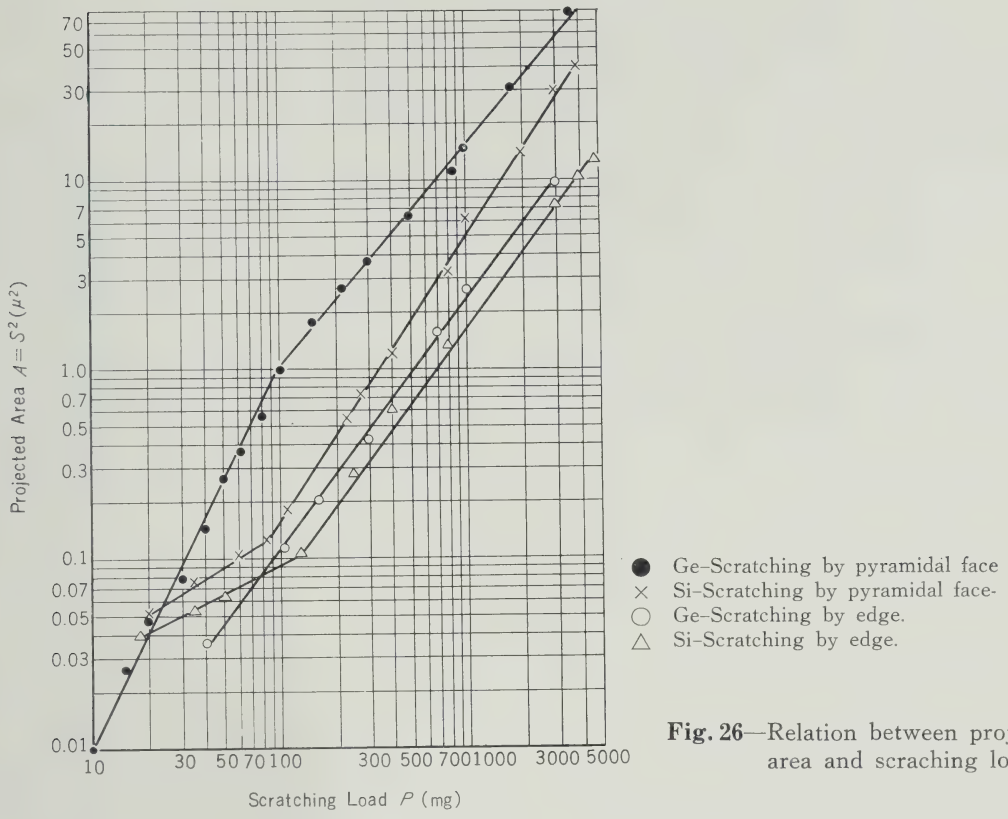

Fig. 26—Relation between projected area and scraching load.

in each case. This, therefore, is the reason why the index n is not constant. The opposite tendency in the first and the second ranges for germanium and silicon is due to the difference of hardness-plasticity. In order words, in the second range where the indenter (pyramid) penetrates the layer to a certain degree of the depth, the inborn low hardness of germanium enables the indenter to cut ma. terials easier, which explains why the width of the scratchings become larger.

In the first range, however the softening is stronger in silicon than in germanium, which yields a similar explanation to the one mentioned above, that the indenter can easily penetrate the layer. However, in the case of work-hardening, the value of n obtained from the scratchings by the edge is proved to be larger. This is because of the more stronger influence of plasticity caused by the restricting condition of the material. If the restriction did not exist, the fracture would be produced and the penetrating action would become larger. This tendency found in the first range of germanium also endorses the above considerations.

Next, for making a comparison between the characteristics of germanium and silicon found in the first range, the relation between the load P and the projected area $A=S^2$ is indicated in Fig. 26. Here, the above raletions are expressed as below.

For scratchings by the pyramidal face on germanium

$$A = 0.0002P^{2.13},$$

for scratchings by the edge on germanium

$$A = 0.0006P^{1.80},$$

for scratchings by the pyramidal face on silicon

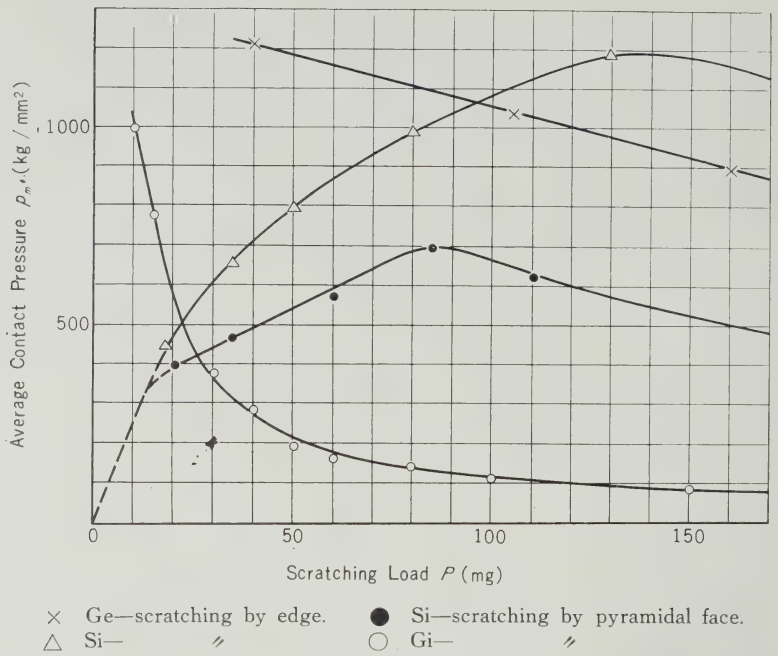

Fig. 27—Relation beetwen average contact pressure and scratching load.

$$A = 0.0022P^{0.74},$$

and for scratchings by the edge on silicon

$$A = 0.0073P^{0.57}.$$

From these results, it is clear that there exists similar plasticity on the surface of silicon as on metal, and less plasticity on the surface of germanium. Conversely saying, it can be said that the softening of silicon enables the surface to be plastic. Then, the above relation is converted to the relation between the load P and the average constant pressure $p_m = P/S^2$, the result of which is indicated in Fig. 27. It is also noticeable that larger plasticity is found in silicon, while it seems to be less in germanium. In the case of perfect plasticity, p_m should be constantly independent of P.[15] However, p_m actually decreases even at a load of 10 mg in germanium, and at a load of over 80 mg in silicon. Though the reason is not fully determined yet, the explanation may be as follows.

The decrease of p_m means the imperfect plasticity of both types of crystals, the cause of which is based upon the size effect of the load P. That is, even though the load is very small, it cannot be said positively that the ultra micro-cracks are not originated entirely in these ranges. In this sense, germanium does not show the plasticity curve yet, which leads to the smaller effect of softening. If the decreasing tendency found in the curve of Fig. 27 is explained by the origination of ultra micro-cracks, p_m will be reduced because of the effective areas when the scratching load increases, or because of the decrease of the average contack pressure itself that comes from the minute change of directions of the intimate contact area, when considering the mean contact pressure as an average of the sum of each pressure on the minute contact areas.

Next, the some estimations are done, because the relation between the average contact pressure and the scratching load seems to indicate the plastic condition in silicon as shown in Fig. 27. That is, the value of a stress at the transition point between the elastic and the plastic region is 340 kg/mm², and the one at the point starting the perfect plasticity is 690

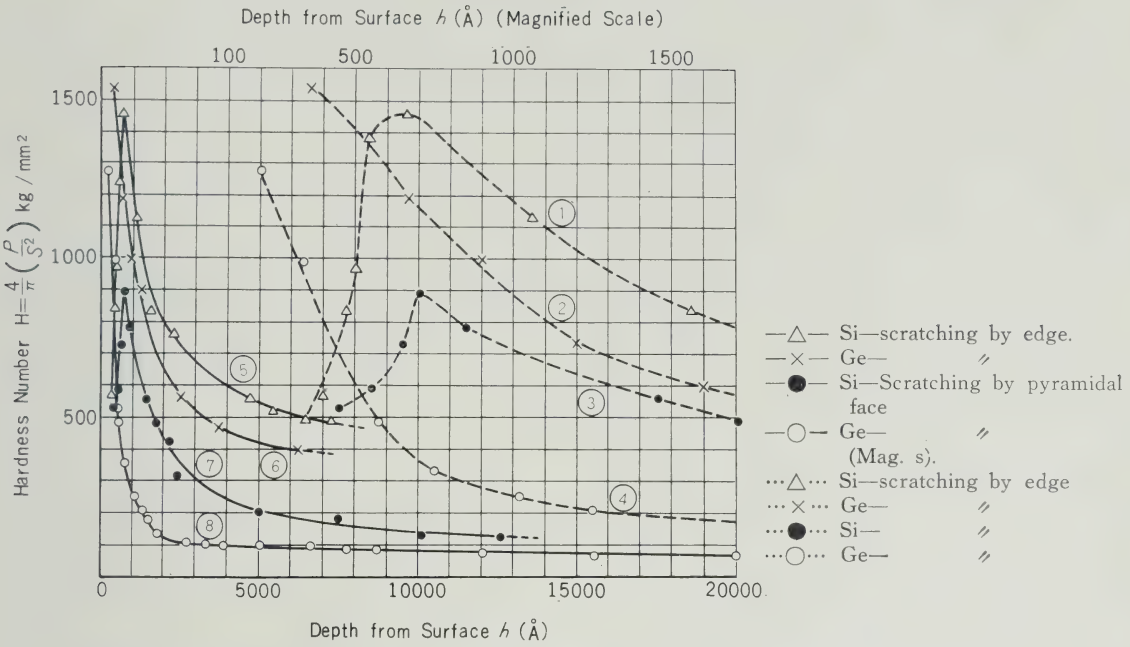

Fig. 28—Hardness distributions on optically polished germanium and silicon.

kg/mm^2 respectively. This ratio becomes 2.8/1.1=2.42 according to the theory of plasticity. Therefore, it can be said that this value agrees with the theoretical one fairly well. Furthermore, the elastic limit, Y, of silicon will be 340/1.1=310 kg/mm^2.

The value mentioned above will be compared with the bending stress of a silicon whisker of 20 μ in diameter, which was reported by Pearson and others.[16] According to their results, the fractured stress is 112 kg/mm^2 at 650° C (the starting point of softening) in silicon. Therefore, the values given here are comparatively higher. However, if the whiskers have the size effect, because diameters of 15 or 20 μ are rather large when considering the theoretical strengths of materials, the larger values mentioned above are not out of reason.

The hardness number, H_s, is obtained along the depths from the surface as illustrated in Fig. 28. From the discussions described above, it can be said that the softening exists in silicon to a depth of 700 Å, while the indication of the softening is seen in germanium at a depth of less than 200 Å. Moreover, the constant hardness numbers are shown at a depth of 10,000–15,000 Å, which is very close to that obtained from the etching rate curves reported in the previous paper.[14] Therefore, the depth mentioned above is considered to be the depth of the total worked or deformed layer caused by optical polishing.

In addition to this, the hardness in the crystal structure is 796 kg/mm^2 for germanium and 1,000 kg/mm^2 for silicon, if the half of the sectional area contributes to the hardness in scratching, that is, the hardness is expressed as $H_s'=4/\pi(P/S^2/2)$. According to the data given by Wang,[8] they are 860 kg/mm^2 and 1,130 kg/mm^2, respectively, so the values obtained here are within reason. Moreover, when calculating the hardness number by using the surface area instead of the projected area, the number becomes 1.5 times larger, that is, 1,000 kg/mm^2 hnd 1,500 kg/mm^2, respectively. These values are larger than those given by Wang. The difference is based upon the fact that the micro-hardness test are performed by using the higher load of at least 10 g, or 50 g in general and that the origination of cracks are overlooked.

Table 2 PHYSICAL AND MECHANICAL PROPERTIES OF VARIOUS MATERIALS

Material	Specific Gravity ρ	Melting Point (° C)	Coefficient of Linear Expansion α ($°C^{-1}$)	Specific Heat C (cal/g·°C)	Thermal Conductivity λ (cal/cm·sec·°C)	Young's Modulus E (kg/mm^2)	Poisson's Ratio ν
Germanium	5.35	960	15×10^{-6}	0.073	0.151	14,100	0.252
Silicon	2.33	1,415	2.3×10^{-6}	0.183	0.270	17,400	0.262
Steel	7.89	1,300–1,400	10×10^{-6}	0.117–0.118	0.161	21,000	0.25–0.33
Quartz	2.65	1,600	7.97×10^{-6}	0.186	0.022	10,400	0.113
Diamond	3.45–3.56	3,500–3,700	1.34×10^{-6}	——	0.33–0.445	90,000	——

4.2. Worked or Deformed Layer from the Thermal Point of View

From the results described in the previous paragraphs, the softening of silicon was considered to be most probable dynamically. If the cause is due to the temperature rise on the surface, the degree of temperature rise should be pursued next.

In optical polishing, there exists a very complicate phenomenon where numerous abrasives are loaded on or embeded into a pitch polisher. However, it is necessary in obtaining a mirror surface to utilize the dry state polishing as described in the previous paper.[14] When considering this state, it may be assumed that polishing consists of a combination of minute contact points, (the area of each point of which is assumed to be that of an abrasive), with the semi-infinite solid surface of the specimen. The relative sliding speed between the abrasive and the specimen is not always the speed of the pitch polisher, because the abrasives roll or slide according to the circumstances. However, the final polishing is in the dry state, and it is passable for abrasives to be embeded in the polisher. Therefore, the sliding speed can be considered the same as that of the pitch polisher. The coefficient of friction is not measured actually, but the coefficient has been determined to be 0.05 for a sapphire stylus on germanium at a load of 0–10 g as described in the previous paragraph 1.3. Further considerations will be given to this coefficient later.

On the assumptions mentioned above, the application of Jaeger's theory will be the best, when considering the moving heat source where the minute contact points become the real heat source on the apparent contact surface having a large area. The temperature rise is then calculated by using the formula below. The results of these measurements on the physical and mechanical properties are given in Table 2 with those of another materials. By the use of numerical values in this table, the temperatures are obtained as follows.

(1) Thermal diffusivity (or thermometric conductivity). K_1 is given as below,

$$K = \frac{\lambda}{c\rho},$$

where λ is thermal conductivity, c specific and ρ density.

Therefore, for silicon and germanium,

$$K_{Si} = 0.640\ \mathrm{cm^2/sec}$$

and

$$K_{Ge} = 0.384\ \mathrm{cm^2/sec}.$$

(2) Non-dimensional number, L, which means the velocity effect, is

$$L = \frac{vl}{2k},$$

where v is the sliding velocity, l the half of length of a square of the heat source. Now, if $v \fallingdotseq 130$ cm/sec and $2l \fallingdotseq 10^{-7}$ nm $= 0.001\ \mu$ (which is inferred from the results of the

electron microscopy for the abrasives and the scratched traces), L is given as below.

$$L_{Si} = 5.1\times10^{-6} < 0.1$$

and

$$L_{Ge} = 8.4\times10^{-6} < 0.1.$$

The above values mean that the velocity effect is small in this case.

(3) The originating calories are determined by replacing the work produced by friction with a thermal one as follows.

$$q = \frac{\mu\cdot W\cdot v}{J\cdot(2l)^2}\ \text{cal/cm}^2\cdot\text{sec},$$

where W is the load supporting the intimate contact area, μ the coefficient of frinction, J the mechanical equivalent of heat.

From the results described in the previous paragraph,

$$W_{Si} = 20\,\text{mg}$$

and

$$W_{Ge} = 15\,\text{mg},$$

(which are obtained from loads showing the cause of the softening). As to the coefficient of friction, the following values are adopted, because the adhesion is considered to be produced more violently in the case of silicon.

$$\mu_{Si} = 0.1$$

and

$$\mu_{Ge} = 0.05.$$

Therefore,

$$q_{Si} = 6.1\times10^{8}\,\text{cal/cm}^2\cdot\text{sec}$$

and

$$q_{Ge} = 2.3\times10^{8}\text{cal/ cm}^2\cdot\text{sec}.$$

(4) The highest temperature on the surface, Θ, is calculated as follows.[15]

$$\Theta = 1.122\times\frac{q\cdot l}{\lambda}\,^\circ\text{C}.$$

Then,

$$\Theta_{Si} = 254^\circ\,\text{C}$$

and

$$\Theta_{Ge} = 170^\circ\,\text{C}.$$

The above values of temperatures are lower than those of the softening points given by Pearson, (which are 650° C and 350° C, respectively). However, it can be said that thermal softening is probably the result of temperature rise on the surface, when it is considered that only a single abrasive is taken into account here. Moreover, the value of μ is 0.05–0.1 now, but the deviation from Amontons's law will occur according to whether or not the penetration of the superficial oxide film is produced, as in the experiments of friction at very light loads described by Whitehead.[18] If the thermal softening is originated, the oxides will be formed on the active surfaces of germanium and silicon.

In fact, the characteristics of the etching rate curves suggested such existence.[14] In the case of surface friction at very low loads, the oxide film may not be penetrated. when considered the results of the ultra microscratchings. Then, whether the coefficient of of friction increases or not depends upon the condition of lubrication on the surface. It appears that the very thin boundary lubricating film is formed by the existence of water acting as the polishing vehicle in the course of the final polishing. The above consideration may be supported by the facts that the adhesion of a specimen to a pitch polisher often occurs if the specimen is left on the pitch polisher even for a very short time, and that the horizontal force of polishing is very large at the final stage. Therefore, the coefficient of friction should be larger at very light loads in polishing, which leads to the tendency of the higher temperature rise.

Next, the point to be considered is the dependence of thermal conductivity on temperature. According to the study by Carruthers and others,[19] it is indicated that the thermal conductivity decreases as the temperature rises. Taking this into account, even though K becomes smaller, L is not so influenced by the decrease of K. However, as seen from the equation determining the highest temperature, Θ becomes higher when λ becomes smaller. Therefore, it can be said that the calculated

values have sufficient meanings in view of the conservative evaluation. As for germanium, the thermal conductivity is measured up to 1020° K by Slack and others.[20] According to them, the thermal conductivity near 300° C becomes one third that at room temperature, which leads to the higher possibility of thermal softening even in germanium.

From the discussions mentioned above, it is concluded that the temperature rise due to surface friction make the surface softer and enable the crystals to be plastic under high pressures at micro-geometric areas, and that the flow takes place, where the mirror surface is formed.

Conclusions

In order to specify the characters of worked layers of optically polished surfaces for semiconductor crystals directly, the ultra micro-scratching hardness tester was constructed, and the relation between the load and the deformation was obtained. Next, the characters of worked layers were discussed in view of the hardness distribution, taking the dynamical and thermal effects into account. The results obtained are summarized as below.

(1) The work softening exists in silicon to a depth of 700 Å, while the indication of softening is seen in germanium at a depth of less than 200 Å.

(2) The constant hardness numbers are found at a depth of 10,000–15,000 Å for both crystals, which is very close to those obtained from the etching rate curves.

(3) The softening phenomenon is caused by the temperature rise due to friction in the course of optical polishing. According to a simplified model, temperatures can be attained up to the softening points for both types of crystals.

(4) The formation of the so-called mirror surface in optical polishing is considered to be produced by microplastic and thermal flow.

Acknowledgement

The authors are indebted to Professor Emeritus, M. Okoshi of Tokyo University for his valuable advice, and to Mr. Y. Nakamura, Associate Director of this Laboratory for his encouragement.

References

(1) I. Ida and Y. Arai, "Comparisons of Characteristics between Optically and Metallographically Polished Surfaces of Semiconductor Crystals," *Rev. Electr. Commun. Labor.* NTT, **10,** 9-10, p. 433, 1962.

(2) D. Tabor, "The Hardness of Metals," Oxford, 1951.

(3) E. Brüche and G. Schimmel, "Über das Ritzen von Glas unter 1 μ Ritzspurbrite," *Glastechn. Ber.*, **27,** 7, S. 239, 1954.

(4) D. Tabor, Mohs' Hardness Scale—A Physical Interpretation," *Proc. Phys. Soc.*, **B67,** p. 249, 1954.

(5) M. S. Alova, "The Anisotropy of Microhardness in Germanium," *Sov. Phys.—Solid State Phys.*, **3,** 6, p. 1320, 1961.

(6) A. A. Giardini, "A Study of the Directional Hardness in Silicon," *Amer. Mineralogist*, **43,** 9-10, p. 957, 1958.

(7) G. C. Kuczynski and R. F. Hochman, "Light-Induced Plasticity in Semiconductors," *Phys. Rev.*, **108,** 4, p. 946, 1957.

(8) C. C. Wang and B. H. Alexander, "Hardness of Germanium-Silicon Alloys at Room Temperature," *Acta Met.*, **3,** p. 515, 1955.

(9) G. C. Kuczynski and R. F. Hochman, "Light-Induced Plasticity in Germanium," *Journ. Appl. Phys.*, **30,** 2, p. 267, 1959.

(10) A. S. Borschcheyskii and N. A. Goriunova, "Study of Microhardness of Certain Semiconductors with the Zinc Blende Structure," *Sov. Phys.—Tech. Phys.*, **2,** 7, p. 1301, 1957.

(11) М. Г. Мильвидскии и Л. В. Лайнер, "Микротвердость и Плотность Дислокаций в Монокристаллах Кремия," Физ. Металл и Металловед., **11,** 6, с. 293, 1961.

(12) M. M. Khrushchov and E. S. Berkovish, "Method of Determining the Hardness of Very Hard Materials" *Ind. Dia. Rev.*, **11,** 2, p. 42, 1951.

(13) M. Okoshi, H. Yoshikawa, and T. Sata, "Grinding Mechanism of a Single Grain," *Journ. of the Soc. for Precision Mechanics in Japan* (*Seimitsu Kikai*), **25,** 6, p. 266, 1957 (in Japanese).

(14) I. Ida, Y. Arai, and M. Suzuki, "Polishing Process and Worked Layers of Semiconductor Crystals," *Rev. Electr. Commun. Labor.*

NTT., 11-12, p. 547, 1962.
(15) F. P. Bowden and D. Tabor, *The Friction and Lubrication of Solids*, Oxford, 1954.
(16) G. L. Pearson *et al*, "Deformation and Fracture of Small Silicon Crystals," *Acta Met.*, **5,** 4, p. 181, 1957.
(17) J. C. Jaeger, "Moving Sources of Heat and Temperature at Sliding Contacts," *Proc. of the Roy. Soc. of New South Wales*, **76,** p. 203, 1942.
(18) J. R. Whitehead, "Surface Deformation and Friction of Metals at Light Loads," *Proc. Poy. Soc.*, **A201,** 1064, p. 109, 1950.
(19) J. A. Carruthers *et al*, "The Thermal Conductivity of Germanium and Silicon between 2° K and 300° K," *Proc. Roy. Soc.* **A238,** p. 502, 1957.
(20) G. A. Slack and C. Glassbrenner, "Thermal Conductivity of Germanium from 3° K to 1020° K," *Phys. Rev.*, **120,** 3, p. 782, 1960.

* * * *

LIST OF THE OFFICIALS OF JAPAN SOCIETY OF CRINDING ENGINEERS (THE 9TH SESSION)

(1963)

Chairman : Dr. Naojiro KUMAGAI (Member of C.I.R.P.)

Secretary : Dr. Akira KOBAYASHI (Member of C.I.R.P.)
Electrotechnical Laboratory, MITI.

Account Auditor : Mr. Hideichi MAKINO
Government Mechanical Laboratory, MITI

Executive Managers : Dr. Norio TAKENAKA
TOKYO University

Dr. Naoharu KINOSHITA
TOYO University

Dr. Ichiro IDA
Electrical Communication Laboratory.

Dr. Osamu IMANAKA
Electrotechnical Laboratory, MITI.

Mr. Tadaaki HANAOKA
CHIBA University.

Mr. Hiroyuki YOSHIKAWA
Institute of Physical and Chemical Research.

Mr. Keizo SHIOMI
NIPPON KOGAKU Co, Ltd.

Mr. Yukio ENDO
KOYO KEMMAZAI Co.,Ltd.

Mr. Kenji SUZUKI
TOYODA Machine Works, Ltd.

Mr. Nakakatsu TAKENO
OKUMA Machinery Works, Ltd.

Mr. Kazuhiko YOKOGAWA
MITSUI Precision Works, Ltd.

UNIVERSITY OF ILLINOIS-URBANA
3 0112 121392259

C O N T E N T S

FEATURES AND PRINCIPLES OF THROUGH WHEEL COOLANT GRINDING.

by Prof. Dr. Kenji SATO

CRITERION OF GRINDING WHEEL TOOL LIFE.

by Hiroyuki YOSHIKAWA

DETERIORATION OF RESINOID GRINDING WHEELS IN GRINDING FLUID.

by Dr. Naoharu KINOSHITA
Tadaaki HANAOKA

MIRROR-FINISH GRINDING BY SELF-SHARPENING OF ABRASIVE GRAINS.

by Kazuhiko YOKOGAWA

WORKED LAYERS OF OPTICALLY POLISHED SURFACES OF SEMICONDUCTOR CRYSTALS VIEWED FROM THE ULTRA MICRO-SCRATCHING HARDNESS.

by Dr. Ichiro IDA
Yuzo ARAI
Makoto SUZUKI